Journal of Sound and Vibration 329 (2010) 5452–5473

Contents lists available at ScienceDirect

Journal of Sound and Vibration

journal homepage: www.elsevier.com/locate/jsvi

A wake oscillator with frequency dependent coupling for the modeling of vortex-induced vibration

R.H.M. Ogink*, A.V. Metrikine

Delft University of Technology, Faculty of Civil Engineering and Geosciences, Stevinweg 1, 2628 CN Delft, The Netherlands

ARTICLE INFO

Article history:
Received 5 February 2010
Received in revised form
4 June 2010
Accepted 8 July 2010
Handling Editor: H. Ouyang
Available online 14 August 2010

ABSTRACT

The aim of this paper is to improve the phenomenological modeling of vortex-induced vibration of an elastically mounted cylinder in fluid flow. To this end an attempt is made to introduce a wake oscillator model that conforms to both the free and forced vibration experiments. This approach is new as in the past wake oscillator models have been tuned to the free vibration experiments only. First, an existing wake oscillator model is improved by properly including the effect of stall and that of the relatively large attack angles in the course of vortex-induced vibration. Then, to comply with the forced vibration experiments, the model is enhanced by introducing frequency dependent coupling. Such a coupling allows reproduction of the measured frequency dependence of the fluid force on the cylinder. The time domain representation of this coupling is a convolution integral. It is found in this paper that if the wake oscillator is modeled with a Van der Pol equation, it is impossible to find one set of frequency dependent coefficients that conforms to the forced vibration experiments at all amplitudes of cylinder motion. Moreover, the frequency dependencies identified for each frequency separately do not seem to satisfy the Kramers–Kronig relations. Based on the above findings, it is concluded that the nonlinearities in the wake oscillator model used in this paper cannot accurately model the results of vortex-induced vibration measurements. The idea proposed in this paper, that a consistent wake oscillator model must conform to the forced vibration experiments as well, is expected to be a powerful tool in the search for the correct nonlinearity.

1. Introduction

Flow over a bluff cylinder separates and vortices will be formed in the wake behind the cylinder. The alternate shedding of these vortices results in an oscillating cross-flow force on the cylinder. The shedding frequency of the vortices follows the Strouhal relation and increases with increasing flow velocity. If the cylinder is mounted flexibly and the frequency of vortex shedding is close to the resonance frequency of the mounted system, the cylinder will start to vibrate in cross-flow direction. With an increase of the flow velocity the vortex shedding frequency no longer follows the Strouhal relation, but locks onto the resonance frequency of the cylinder, thereby sustaining violent vibration of the cylinder over a wide range of flow velocities. This phenomenon is known as vortex-induced vibration (VIV). The occurrence of VIV can cause severe problems for long cylindrical structures that are exposed to air or water flow such as chimneys, railroad contact wires, the

* Corresponding author. Tel.: +31 15 2789225; fax: 031 15 2785767.
E-mail address: richard@richardogink.net (R.H.M. Ogink).

0022-460X/$ - see front matter © 2010 Elsevier Ltd. All rights reserved.
doi:10.1016/j.jsv.2010.07.008

cables of stay bridges and free-hanging offshore pipelines. Recent reviews on VIV have been given by Sarpkaya [1] and Williamson and Govardhan [2].

Ideally, one would like to analyze VIV by solving the equations of structural motion coupled to the fully nonlinear equations of fluid flow. For the cases of VIV that are encountered by design engineers, this would entail solving the equations of fluid flow at high Reynolds numbers for flow patterns that are partially or fully turbulent. The numerical treatment of turbulent and high Reynolds number flows is however exceedingly difficult and, additionally, for long cylindrical structures full numerical analysis of the fluid flow along the length of the structure would be computationally too expensive, especially when dozens of current speeds and directions have to be analyzed. Engineers therefore rely on semi-empirical models. Two models that are often used are the force-decomposition model and the wake oscillator model. For a review on VIV modeling see Gabbai and Benaroya [3].

In the force-decomposition model, originally based on the work of Sarpkaya [4], measured fluid forces are directly used as forcing terms in the equation of structural motion. These fluid forces are measured in so-called forced vibration experiments, in which a rigid cylinder placed in a fluid flow is forced to vibrate harmonically over a range of amplitudes and frequencies. The measured fluid force is then decomposed in a part in phase with the cylinder acceleration, which acts as an added mass, and a part in phase with the cylinder velocity, which acts as an added damping. By applying the measured forces as forcing terms in the equation of structural motion, sustained vibration can be predicted for the range of flow velocities in which the fluid added damping is negative. The amplitude and frequency of vibration are found through an iterative procedure. The advantage of the force-decomposition method is that one can measure the fluid forces for specific cases, such as for instance at a certain Reynolds number or for a certain cylinder roughness, and then apply the measured forces in a direct manner. The disadvantage of this method is however that for long flexible cylindrical structures the response due to vortex shedding may contain contributions from several standing and travelling waves [5,6]. In this case the spectrum of vibration of each segment of the structure contains several frequencies and a dominant frequency should be chosen for the successful application of the method. In many cases the latter is impossible. Moreover, it is unlikely that a vibratory pattern containing multiple frequencies can be predicted accurately by using fluid forces that have been measured at a single frequency.

A second type of semi-empirical model that is used to describe VIV is the wake oscillator. Instead of direct application of measured fluid forces to the equation of structural motion, wake oscillator models couple the equation of structural motion with a nonlinear oscillator equation that describes the cross-flow fluid force. In most cases an equation of the Van der Pol or Rayleigh type is used, as these equations predict a limit cycle in the phase space. A Van der Pol equation that could be used is

$$\ddot{C}_y+\varepsilon\omega_s\dot{C}_y\left(C_y^2-\frac{1}{4}\hat{C}_{y1}^2\right)+\omega_s^2C_y=f(Y,\dot{Y},\ddot{Y}), \tag{1}$$

where C_y is the nondimensional cross-flow fluid force, $\hat{C}_{y1}$ is the amplitude of the limit cycle of the unforced oscillator, ω_s is the vortex shedding frequency, ε is a nondimensional tuning parameter and overdots denote derivatives with respect to time. The right-hand side of Eq. (1) models the coupling between the structural displacement Y and the fluid. When Eq. (1) is coupled to the equation of structural motion and the system is solved in the time domain, it is found that for a range of flow velocities, this model predicts a cylinder motion with the cross-flow fluid force locked onto it. The merit of the wake oscillator compared to the force-decomposition method is that there is no assumption of a single dominant frequency of motion. The model finds the frequency and amplitude of the cylinder motion and the cross-flow fluid force on its own accord. This makes it possible to use this model to describe multimode VIV of long flexible cylinders. Wake oscillator models have been used to model vortex-induced vibration of flexible structures in [7,8]. The disadvantages of the wake oscillator model are however that the model is phenomenological in nature and that there are no direct methods to derive the nonlinearity and the coupling term in Eq. (1). Therefore, all wake oscillator models contain tuning parameters to adjust the model to the results of experiments. Even though a considerable number of wake oscillator models have been developed, a more detailed discussion will follow in Section 3.1, the correspondence between model predictions and VIV measurements is in most cases approximate at best. The main problem is to find a model that can describe at the same time both the correct range of flow velocities, in which lock-in takes place, and the correct amplitude of cylinder motion.

In this paper, to improve the concept of the oscillator model it is proposed to make the coupling term in Eq. (1) frequency dependent. It should be possible to achieve this by tuning this coupling term for each frequency separately to the forced vibration measurements. By using an appropriate transform the frequency dependent coupling can be written as a convolution integral in the time domain. In this way the model can still be used in the time domain without having to specify the frequency of vibration in advance, thereby leaving intact the most attractive feature of the wake oscillator model.

It is well known that in the description of fluid–structure interaction the fluid added mass and fluid added damping can be frequency dependent. In the description of ship motions, for example, the convolution integral formulation, introduced by Cummins in 1962 [9], is often used. Whereas in ship hydromechanics the equations are linear, the novelty in the application to wake oscillators is that the frequency dependence will be introduced into a nonlinear equation. As shown in this paper, this can be used to check whether the nonlinear oscillator equation contains the correct nonlinearities by way of comparing model predictions with measurements.

The main ambition of this paper is to formulate a new wake oscillator model that is capable of describing both forced and free vibration experiments. This will be achieved by including convolution integrals into the model and determining

the kernels of these integrals on the basis of forced vibration experiments. This will make it possible to tune the wake oscillator to specific forced vibration datasets for example for different Reynolds number regimes.

As the forced vibration measurements of Gopalkrishnan [10] and the free vibration measurements of Khalak and Williamson [11] have been conducted in approximately the same Reynolds number regime, the frequency dependent coupling will be determined on the basis of these measurements. Therefore, Section 2 starts with a short description of these experiments. In Section 3, the fundamentals of the oscillator model that will be used in this paper will be described. The frequency dependent coupling and the necessary transform techniques are explained in Section 4. In the section thereafter these methods are applied for prediction of the free vibration experiments and the results are compared with the measurements. Finally, in Section 6 concluding remarks are given.

2. Experimental quantification of vortex-induced vibration

Two types of experiments can be carried out to investigate VIV of a rigid cylinder. These are the so-called free vibration and forced vibration experiments. In free vibration experiments the cylinder is placed in a wind tunnel or water channel and is free to vibrate in cross-flow direction at an amplitude and frequency determined by the system, while in forced vibration experiments fluid forces are measured on a cylinder that is forced to vibrate with a certain amplitude and frequency.

2.1. Free vibration experiments

Results of free vibration experiments have been reported in the literature by Feng [12], Hover et al. [13], Khalak and Williamson [11,14,15] and Klamo et al. [16,17]. During a typical free vibration experiment the cross-flow displacement Y of an elastically mounted cylinder is measured at a certain flow velocity V. From the resulting time series the recurrent maximum displacement $\hat{Y}_{\max}$ and dominant frequency of cylinder motion ω_c can be determined. The experiment is then repeated over a range of flow velocities. Usually the results are presented as graphs, in which the nondimensional amplitude and frequency are plotted versus the reduced velocity V_n. In these graphs the amplitude $\hat{Y}_{\max}$ is made nondimensional by dividing it by the cylinder diameter D. For experiments performed in water, the frequency ω_c is made nondimensional by dividing it by the system natural frequency in water ω_n, which is given by $\omega_n=2\pi f_n=(k/(m+m_a))^{1/2}$. In the preceding equation, k is the spring stiffness of the suspension system, m the cylinder mass and $m_a=\hat{C}_a\pi\rho D^2L/4$ the added mass, in which ρ denotes the density of the fluid and L the cylinder length. The value for the coefficient $\hat{C}_a$ is taken as 1.0 from potential theory. The reduced velocity V_n is defined as $V_n=V/D/f_n$. The results of free vibration experiments depend on the mass and damping ratios of the test setup [14,15,17]. The mass ratio m^* and the damping ratio in water ζ are defined as

$$m^*=\frac{m}{\frac{\pi}{4}\rho D^2L},\quad \zeta=\frac{b}{2\omega_n(m+m_a)}=\frac{b}{2\sqrt{k(m+m_a)}}. \tag{2}$$

Generally speaking, the mass ratio m^* of experiments conducted in air is high and that of experiments conducted in water low. In this paper only the results of experiments conducted in water will be used.

As explained in the introduction, predictions of the wake oscillator model will be compared with the free vibration measurements of Khalak and Williamson. In their experiments an elastically mounted circular cylinder was placed in a water channel and allowed to vibrate freely in cross-flow direction. The amplitude and frequency ratio for three of their experiments, based on Fig. 6 in [11], are plotted in Fig. 1a–c. The mass and mass-damping ratios of these experiments were, respectively, $m^*=2.4$, $m^*\zeta=0.014$; $m^*=10.3$, $m^*\zeta=0.017$ and $m^*=20.6$, $m^*\zeta=0.029$. The Reynolds number was in the range of 3500–10 000. Khalak and Williamson found that for low mass-damping the amplitude plot contains 3 branches. They named these branches, in order of increasing reduced velocity, the initial, upper and lower branch. The branches have been labeled IB, UB and LB, respectively, in Fig. 1a–c. The nondimensional amplitude of the cylinder motion in these experiments was around 0.9 for the upper branch and 0.6 for the lower branch. Khalak and Williamson [11,15] found that the jump between the initial and the upper branch is hysteretic, while the transition from the upper to the lower branch takes place via an intermittent switching. Regarding the periodicity of the cylinder motion, they report in [14] that in the initial and upper branch the motion is quasi-periodic, being a combination of frequencies, while in the lower branch the motion is nearly periodic, containing only one dominant frequency. Finally, it can clearly be seen in Fig. 1 that when the mass ratio is reduced the lock-in range increases.

2.2. Forced vibration experiments

Forced vibration experiments have been conducted by, among others, Bishop and Hassan [18,19], Mercier [20], Sarpkaya [4], Staubli [21], Wu [22] and Gopalkrishnan [10]. Typically, for forced vibration experiments, the Fourier coefficients of the in-line and cross-flow forces are determined at the frequency of forced vibration, as it is assumed that during lock-in the fluid forces oscillate at the frequency of cylinder motion. Most researchers plot their results as function of the frequency of forced vibration f_c or ω_c or as function of the reduced velocity V_c that is based on this frequency of forced vibration, i.e. $V_c=V/D/f_c$. For each Fourier coefficient a number of curves are given, one for each amplitude of forced vibration.

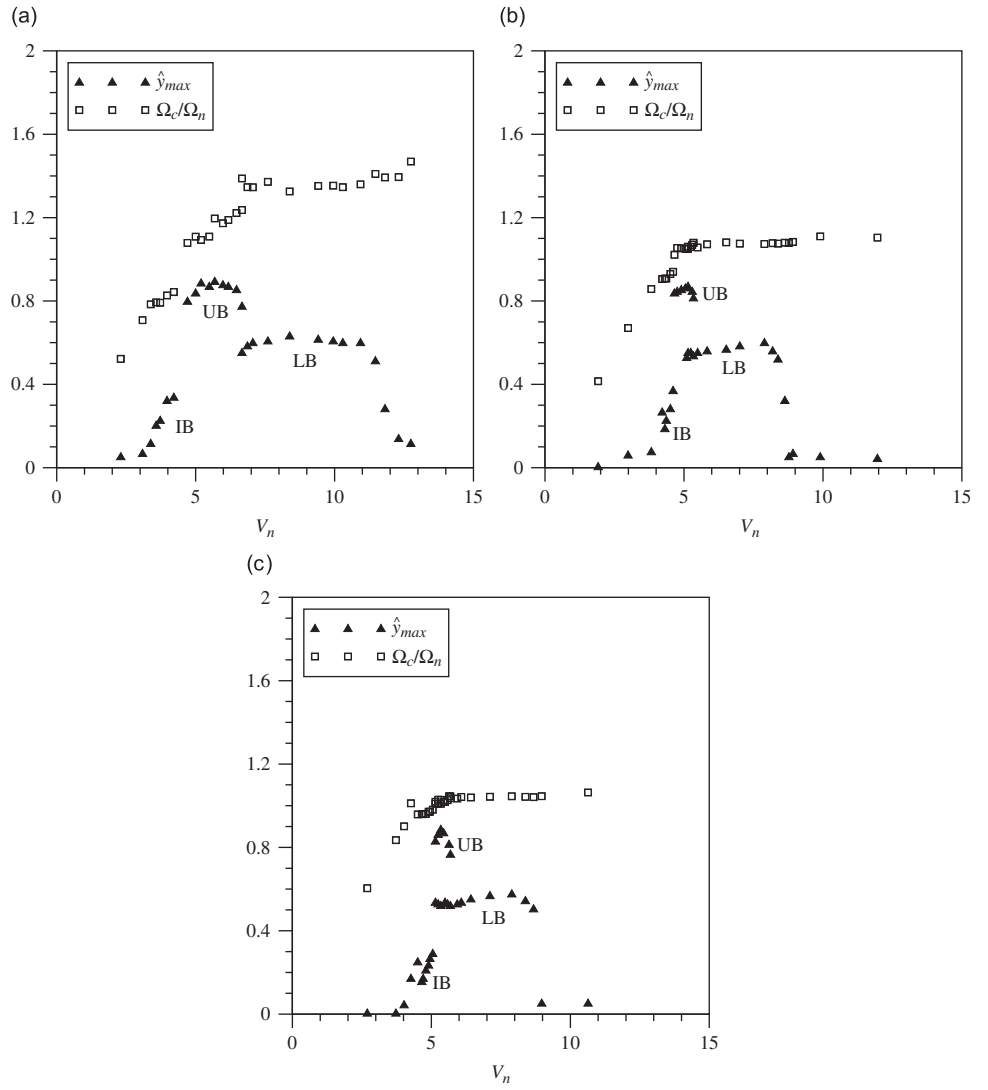

Fig. 1. Amplitude and frequency of cylinder motion from the measurements of Khalak et al. [11] for: (a) m^*=2.4, (b) m^*=10.3 and (c) m^*=20.6.

Unfortunately, nearly every researcher uses his/her own notation to denote the coefficients, making it at times difficult to compare results of different groups. The following notation is used consistently in this paper. Processed coefficients and amplitudes carry a circumflex to distinguish them from the time series. Forced vibration experiments have a superscript '0' or 'y', where '0' is used for the stationary cylinder and 'y' for the cylinder forced to vibrate in the vertical y-direction. Subscripts 'x' and 'y' give the direction of the force component. Processed coefficients carry a second subscript which denotes the harmonic component for which the Fourier coefficient has been determined. For the stationary cylinder the fundamental frequency is the Strouhal frequency, for the forced vibration the fundamental frequency is the frequency of forcing. The third subscript indicates the phasing of the coefficient, that is, 'sin' and 'cos' denote whether a sine or cosine integral has been used to determine the Fourier coefficient. The other option for the third subscript is that 'a' and 'v' are used to denote the coefficient in phase with the cylinder acceleration and that in phase with the cylinder velocity, respectively. It is always assumed that the forced cylinder motion is given by $Y=\hat{Y}\sin(\omega_c t)$. As an example, $\hat{C}^y_{x2\cos}$ has a superscript 'y' to represent the results of a cross-flow forced vibration experiment, a subscript 'x' to represent the in-line force, a subscript '2' to represent the second harmonic and a subscript 'cos' to represent computation with a cosine integral.

All fluid forces are made nondimensional in the usual manner: $C=F/(\frac{1}{2}\rho DV^2L)$. For the stationary cylinder (Y=0) the oscillating cross-flow force $\hat{C}^0_{y1}$ and the mean in-line force $\hat{C}^0_{x0}$ are given by

$$\hat{C}^0_{y1\sin}=\frac{2}{T_s}\int_{t_0}^{t_0+T_s} C^0_y\sin(\omega_s t)\,\mathrm{d}t,\quad \hat{C}^0_{y1\cos}=\frac{2}{T_s}\int_{t_0}^{t_0+T_s} C^0_y\cos(\omega_s t)\,\mathrm{d}t,$$

$$\hat{C}^0_{y1} = \sqrt{\hat{C}^0_{y1\sin}2 + \hat{C}^0_{y1\cos}2},$$
$$\hat{C}^0_{x0} = \frac{1}{T_s}\int_{t_0}^{t_0+T_s} C^0_x \, \mathrm{d}t, \tag{3}$$

where $T_s = 2\pi/\omega_s$. For the cylinder forced to vibrate as $Y = \hat{Y}\sin(\omega_c t)$, the component of the cross-flow force in phase with the cylinder acceleration $\hat{C}^y_{y1a}$, in phase with the cylinder velocity $\hat{C}^y_{y1v}$ and the mean in-line force $\hat{C}^y_{x0}$ are defined as

$$\hat{C}^y_{y1a} = \frac{2}{T_c}\int_{t_0}^{t_0+T_c} C^y_y \sin(\omega_c t)\,\mathrm{d}t, \quad \hat{C}^y_{y1v} = -\frac{2}{T_c}\int_{t_0}^{t_0+T_c} C^y_y \cos(\omega_c t)\,\mathrm{d}t,$$
$$\hat{C}^y_{x0} = \frac{1}{T_c}\int_{t_0}^{t_0+T_c} C^y_x \, \mathrm{d}t, \tag{4}$$

The most complete set of forced vibration measurements that is publically available is the one that has been published by Gopalkrishnan [10]. His test setup consisted of a horizontal cylinder that was pulled through a water channel, while being forced to oscillate sinusoidally in vertical direction. He measured the fluid forces on the cylinder for 51 nondimensional frequencies f_cD/V ranging from 0.05 to 0.35 and for 6 nondimensional amplitudes $\hat{y}$ ranging from 0.15 to 1.2. The Reynolds number of his experiment was around 10 000. In [10] he provides, besides the force coefficients for the stationary cylinder, the contour plots of $\hat{C}^y_{x0}$, $\hat{C}^y_{x2}$, $\hat{C}^y_{y1a}$ and $\hat{C}^y_{y1v}$. A more detailed contour plot of $\hat{C}^y_{y1a}$ and $\hat{C}^y_{y1v}$ based on the same set of measurements has been given by Hover et al. in [13]. The contour plots of $\hat{C}^y_{x0}$, $\hat{C}^y_{y1a}$ and $\hat{C}^y_{y1v}$ have been read for the amplitudes $\hat{y}$=0.2, 0.4, etc. till 1.2 by magnifying the plots from [10,13], linearly interpolating between the lines of the contour plot and then smoothing the curves that have been obtained for each amplitude with a cubic spline approximation. The curves that have been read in this manner for $\hat{C}^y_{y1a}$, $\hat{C}^y_{y1v}$ and $\hat{C}^y_{x0}$ are depicted in Fig. 2. Note that the amplitudes at which the contour plots have been read, are not necessarily the amplitudes at which Gopalkrishnan has performed his measurements. Obviously, our reading of the plots cannot have been perfect, but the curves that have been obtained are accurate enough for our purposes.

3. The wake oscillator

3.1. The concept of the wake oscillator

The notion of the wake oscillator has been introduced by Birkhoff [23] and Birkhoff and Zarantonello [24]. He noted that 'the wake swings from side to side, somewhat like the tail of a swimming fish.' He described the motion of the angle between wake axis and incoming flow with a linear oscillator. His intention was to find expressions for the Strouhal frequency and vortex spacing in the wake and not so much to determine the cross-flow fluid force. Bishop and Hassan [19] noted as well that the wake seems to behave as an oscillator. They stated in their paper concerning their forced vibration experiments that 'lift and drag forces responded to forcing rather as a simple oscillator would under similar circumstances.'

Among the first researchers to use a nonlinear oscillator equation to model the cross-flow force and to couple this oscillator to the structural equation of motion are Hartlen and Currie [25] and Skop and Griffin [26] and Griffin et al. [27]. Hartlen and Currie used a Rayleigh equation and Skop and Griffin a Van der Pol equation like Eq. (1). The Rayleigh equation is very similar to the Van der Pol equation, except that the generalized damping term is $\varepsilon\omega_s\dot{C}_y(\dot{C}_y^2 - \frac{3}{4}\omega_s^2\hat{C}_{y1}^2)$ instead of $\varepsilon\omega_s\dot{C}_y(C_y^2 - \frac{1}{4}\hat{C}_{y1}^2)$. In both the Rayleigh and the Van der Pol equation the generalized damping term is negative for small motion and positive for large motion. So, at small amplitudes of motion there is energy input and at larger amplitudes there is energy dissipation. Therefore these equations predict a limit cycle. By coupling the nonlinear oscillator to the equation of motion through the right-hand side of Eq. (1), the lock-in of the cross-flow force can be modeled. Both the model of Hartlen and Currie as well as of Skop and Griffin deviate from the original idea of Birkhoff by using the cross-flow force as the variable in the nonlinear oscillator, instead of the wake angle.

A considerable number of wake oscillator models can be found in the literature on vortex-induced vibration. Nakamura [28] and Tamura and Matsui [29] continue along the lines of Birkhoff by deriving a model based on the wake angle. The model of Iwan and Blevins [30] is notable as it is derived from cross-flow momentum considerations. Landl [31] and Berger [32] developed models that contain higher order nonlinearities in the damping term of the wake oscillator and Krenk and Nielsen [33] developed a model that combines the nonlinearities of the Van der Pol and the Rayleigh equation.

Two important insights on the workings of the wake oscillator model have been provided by Skop and Balasubramanian [34] and Facchinetti et al. [35]. Skop and Balasubramanian included a stall term in the description of the cross-flow force. The stall term is dependent on the cylinder velocity and models the cross-flow fluid added damping. This results in an equation for the cross-flow force of the following form: $C_y = c_1 q + c_2\dot{Y}$, in which c_1 and c_2 are constants and q is now the oscillating wake variable that is the unknown function in either a Van der Pol or Rayleigh equation. In the next subsection it will be shown that correct inclusion of the stall term facilitates tuning of the wake oscillator considerably. Facchinetti et al. systematically investigated the form of the forcing by the cylinder motion on the wake oscillator. They looked at a

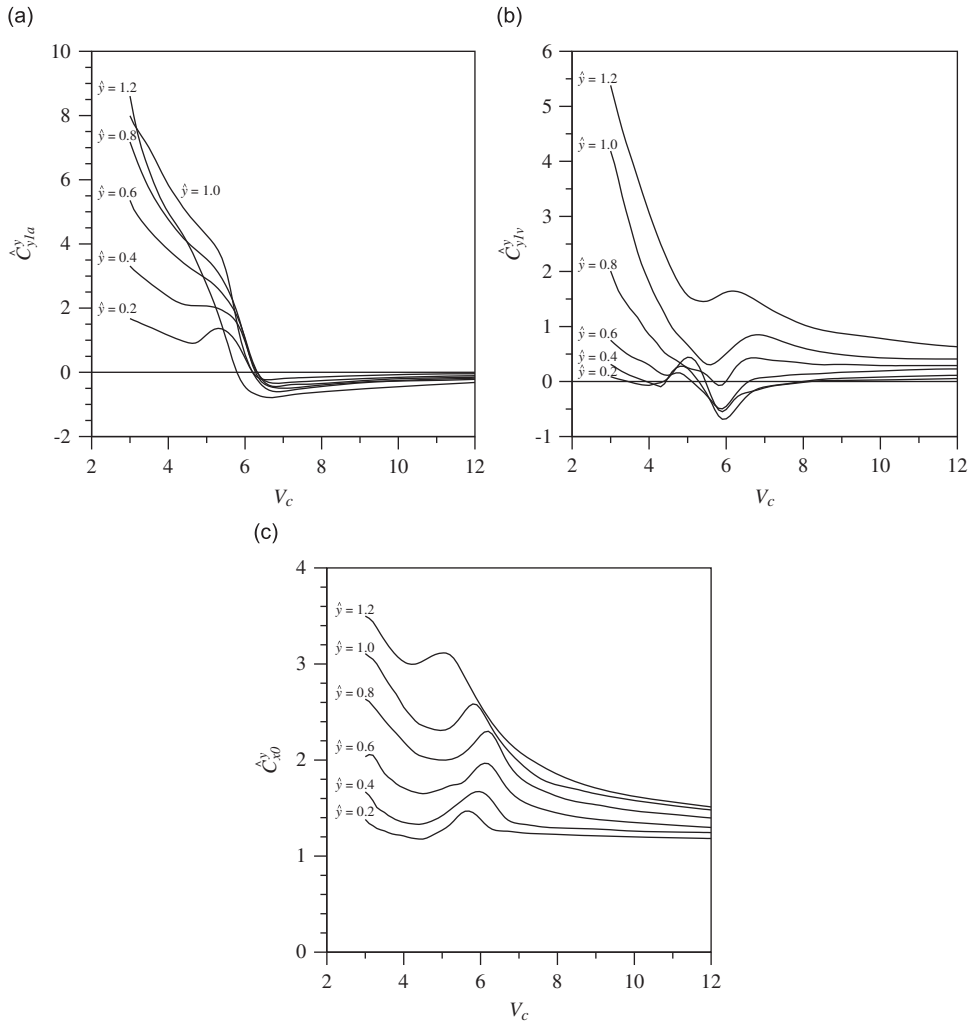

Fig. 2. Fluid force coefficients from the measurements of Gopalkrishnan [10] of: (a) the cross-flow force component in phase with the cylinder acceleration ($\hat{C}^y_{y1a}$), (b) the cross-flow force component in phase with the cylinder velocity ($\hat{C}^y_{y1v}$) and (c) the mean in-line force ($\hat{C}^y_{x0}$).

displacement, velocity and acceleration coupling and found that the acceleration coupling models the lock-in domain best. In a follow-up paper De Langre [36] showed that the instability found by coupling two oscillators through an acceleration coupling, is in fact coupled mode flutter and that coupled mode flutter is therefore the explanation (of the lower branch) of the lock-in domain.

The wake oscillator model that will be made frequency dependent will be based on the model of Facchinetti et al. [35]. Therefore a description of this model will be given in the next subsection. Along the way, this model will be adjusted and retuned to better suit the purposes of this paper.

3.2. The model of Facchinetti, De Langre and Biolley

3.2.1. Derivation of the original model along the lines of Facchinetti et al.

In dimensional form, Facchinetti et al. start with the following set of equations:

$$(m+m_a)\frac{d^2Y}{dt^2}+b\frac{dY}{dt}+kY=\frac{1}{2}\rho DV^2LC_{VY}, \tag{5}$$

$$\frac{d^2q}{dt^2}+\varepsilon\omega_s(q^2-1)\frac{dq}{dt}+\omega_s^2q=\frac{A}{D}\frac{d^2Y}{dt^2}, \tag{6}$$

where q is the wake variable and ω_s the Strouhal frequency. This frequency is given by the relation $\omega_s=2\pi$ St V/D, where St denotes the Strouhal number. The parameters A and ε are tuning parameters. The coupling term on the right-hand side of Eq. (6) is an acceleration coupling as mentioned before. The total cross-flow force is assumed to consist of a vortex force

F_{VY} due to vortex shedding and a potential added mass force F_{AY}:

$$F_y = F_{VY} + F_{AY} = \frac{1}{2}\rho D V^2 L C_{VY} - m_a \frac{\mathrm{d}^2 Y}{\mathrm{d}t^2}. \tag{7}$$

Following the model of Skop and Balasubramanian, Facchinetti et al. assume that the cross-flow vortex force C_{VY} is composed of a part determined by the wake oscillator and a part due to stall. They refer to Blevins [37], who, for galloping, decomposes the cross-flow force C_{VY} into a drag part C_{VD} and a lift part C_{VL}, where drag and lift are defined as, respectively, being in-line with and perpendicular to U, which is the total velocity relative to the moving cylinder. Now, assuming this decomposition to be valid for vortex-induced vibration as well, then C_{VL} should be related to the wake variable q and C_{VD} to the stall term. The decomposition of C_{VY} is given by

$$C_{VY} = (C_{VD}\sin\beta + C_{VL}\cos\beta)\frac{U^2}{V^2} \quad \text{with } U = \sqrt{V^2 + \left(\frac{\mathrm{d}Y}{\mathrm{d}t}\right)^2}, \tag{8}$$

in which β is the angle between the directions of U and the undisturbed flow velocity V. The angle β and the decomposition of C_{VY} into C_{VD} and C_{VL} are depicted in Fig. 3. The angle β is given by

$$\beta = -\arctan\left(\tfrac{\mathrm{d}Y}{\mathrm{d}t}/V\right), \quad \sin\beta = -\tfrac{\mathrm{d}Y}{\mathrm{d}t}/U = -\tfrac{\mathrm{d}Y}{\mathrm{d}t}/\sqrt{V^2 + \left(\tfrac{\mathrm{d}Y}{\mathrm{d}t}\right)^2},$$
$$\cos\beta = V/U = V/\sqrt{V^2 + \left(\tfrac{\mathrm{d}Y}{\mathrm{d}t}\right)^2}. \tag{9}$$

Because Facchinetti et al. were interested in studying the fundamental behavior of the coupling between Eqs. (5) and (6) analytically, they linearized Eq. (8) by assuming that the cylinder velocity is much smaller than the flow velocity and that therefore the angle β is much smaller than 1. Hence:

$$\frac{\mathrm{d}Y}{\mathrm{d}t} \ll V, \quad \text{so that } \sin\beta \approx \beta \approx -\frac{1}{V}\frac{\mathrm{d}Y}{\mathrm{d}t}, \quad \cos\beta \approx 1 \tag{10}$$

$$\text{and} \quad C_{VY} \approx \left(-\frac{1}{V}\frac{\mathrm{d}Y}{\mathrm{d}t}C_{VD} + C_{VL}\right). \tag{11}$$

By replacing C_{VY} on the right-hand side of Eq. (5) by Eq. (11), one sees that the stall term in the model of Facchinetti et al. is given by $-(1/V)(\mathrm{d}Y/\mathrm{d}t)C_{VD}$.

The problem statement is made nondimensional using the following equalities:

$$\tau = \omega_s t, \quad \mathcal{T} = \omega_s T, \quad \Omega = \frac{\omega}{\omega_s} = \frac{f}{f_s}, \quad y = \frac{Y}{D}. \tag{12}$$

The reduced velocities are then given by $V_n = 1/\mathrm{St}/\Omega_n$ and $V_c = 1/\mathrm{St}/\Omega_c$ and substitution of (12) into Eqs. (5) and (6) results in

$$\ddot{y} + 2\zeta\Omega_n\dot{y} + \Omega_n^2 y = \frac{\rho D^2 L}{(m+m_a)}\frac{1}{8\pi^2\,\mathrm{St}^2}C_{VY}, \tag{13}$$

$$\ddot{q} + \varepsilon(q^2-1)\dot{q} + q = A\ddot{y} \tag{14}$$

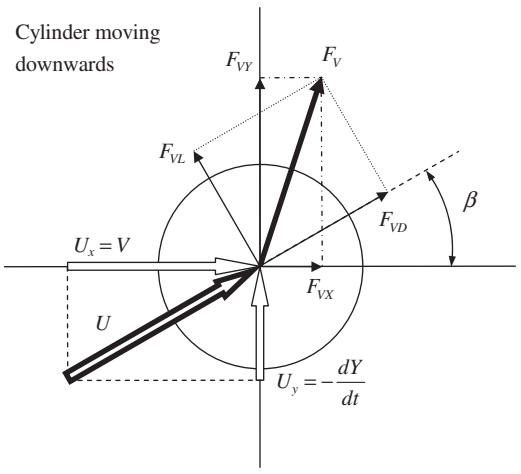

Fig. 3. Definition of the angle β and the decomposition of the vortex fluid force in drag, lift, horizontal and vertical direction.

with the reduced damping $\zeta = b/(2\omega_n(m+m_a))$ and natural frequency $\Omega_n = (k/(m+m_a))^{1/2}/\omega_s$, both defined as in Section 2.1 on the basis of the mass and added mass combined. From hereon overdots will denote derivatives with respect to nondimensional time τ. In nondimensional form the nonlinear equations for the angle β and the cross-flow force C_{VY} are given by Eqs. (15) and (16) and after linearization by Eqs. (17) and (18):

$$\sin\beta = \frac{-2\pi\,\mathrm{St}\,\dot{y}}{\sqrt{1+(2\pi\,\mathrm{St}\,\dot{y})^2}}, \quad \cos\beta = \frac{1}{\sqrt{1+(2\pi\,\mathrm{St}\,\dot{y})^2}}, \tag{15}$$

$$C_{VY} = (-2\pi\,\mathrm{St}\,\dot{y}C_{VD} + C_{VL})\sqrt{1+4\pi^2\,\mathrm{St}^2\,\dot{y}^2}, \tag{16}$$

$$\sin\beta = -2\pi\,\mathrm{St}\,\dot{y}, \quad \cos\beta = 1, \tag{17}$$

$$C_{VY} = (-2\pi\,\mathrm{St}\,\dot{y}C_{VD} + C_{VL}). \tag{18}$$

All that now remains to complete the model is to couple C_{VY} to the wake variable q. Facchinetti et al. assume that the drag component of the vortex force is constant and that the lift component of the vortex force is linearly related to the wake variable q. For a stationary cylinder, $C_{VD}=C_{VX}$ and $C_{VL}=C_{VY}$, as $\beta=0$. This means that C_{VD} should be equal to the constant in-line force coefficient measured for a stationary cylinder and that C_{VY} should be equal to the oscillating cross-flow coefficient measured for a stationary cylinder:

$$C_{VD} = \hat{C}^0_{x0}, \quad C_{VL} = \frac{\hat{C}^0_{y1}}{\hat{q}_1}q, \tag{19}$$

where $\hat{q}_1$ is the amplitude of the limit cycle of the unforced wake oscillator, so that $q/\hat{q}_1$ oscillates between 1 and -1. For the Van der Pol equation $\hat{q}_1 = 2$. After performing the necessary substitutions into Eq. (13), the equation of structural motion is finally given in nonlinear form by Eq. (20) and after linearization by Eq. (21):

$$\ddot{y} + 2\zeta\Omega_n\dot{y} + \Omega_n^2 y = \frac{\rho D^2 L}{(m+m_a)}\frac{1}{8\pi^2\,\mathrm{St}^2}\left(-2\pi\,\mathrm{St}\,\dot{y}\hat{C}^0_{x0} + \frac{\hat{C}^0_{y1}}{\hat{q}_1}q\right)\sqrt{1+4\pi^2\,\mathrm{St}^2\,\dot{y}^2}, \tag{20}$$

$$\ddot{y} + \left(2\zeta\Omega_n + \frac{\rho D^2 L}{(m+m_a)}\frac{\hat{C}^0_{x0}}{4\pi\,\mathrm{St}}\right)\dot{y} + \Omega_n^2 y = \frac{\rho D^2 L}{(m+m_a)}\frac{1}{8\pi^2\,\mathrm{St}^2}\frac{\hat{C}^0_{y1}}{\hat{q}_1}q. \tag{21}$$

3.2.2. Significance of linearization in the original model of Facchinetti et al.

The original model of Facchinetti et al., consisting of Eqs. (21) and (14), needs as input the cylinder and spring parameters m, k, b, D and L and the flow parameters ρ and V. To tune the model to the results of a certain experiment, one would ideally want to use the values for $\hat{C}^0_{x0}$, $\hat{C}^0_{y1}$ and St as they have been measured within this experiment. This leaves only the parameters A and ε truly free to tune the model. Facchinetti et al. use $\hat{C}^0_{y1}=0.3$, St=0.2 and $\hat{C}^0_{x0}=2.0$. They acknowledge that for $\hat{C}^0_{x0}$ a value of approximately 1.2 is found in the literature, but they need to set $\hat{C}^0_{x0}$ at a higher value because of the small angle assumption, as this assumption reduces the fluid added damping. They proceed by deriving that the lift magnification factor is a function of A/ε and on the basis of a set of published measurements set this ratio at 40. Finally they choose $A=12$ and $\varepsilon=0.3$ by comparing the lock-in range of their model with measurements.

To facilitate the incorporation of frequency dependent effects into the model, it is first tested whether the wake oscillator model as it is described above needs additional fine-tuning and whether the linearization of C_{VY} has a large influence on the model results. Predictions of the model, with the parameters of Facchinetti et al., are therefore compared in Fig. 4a and b with the free vibration measurements of Khalak et al. for $m^*=10.3$ and $m^*=20.6$.

The coupled system, consisting of Eqs. (21) and (14), has been solved numerically, using a fifth order Runge–Kutta routine. The system is integrated in time at a certain reduced velocity V_n with a time step of $d\tau = \mathcal{T}_n/100$. The cylinder response $y(\tau)$ reaches a steady state after just a few periods of oscillation, but analysis of the response starts only after 50 periods. Then, for a time series with a length of 50 periods, $\hat{y}_{\max}$ is determined by finding the maximum recurrent displacement and Ω_c is found by determining the highest peak in the Fourier spectrum of the analyzed time series. The amplitude and frequency are determined in the range $V_n=2$–12, with a stepsize of $dV_n=0.1$. The initial conditions that have been used for $V_n=2$ are: $y(0)=\dot{y}(0)=\dot{q}(0)=0$ and $q(0)=0.01$. Then, for all other reduced velocities, the last values of y, $\dot{y}$, q and $\dot{q}$ in the time series of the preceding reduced velocity have been used as the initial conditions of the following reduced velocity. To search for hysteresis all calculations have been performed twice. Once with the initial conditions taken from the last lower reduced velocity and once in backward direction with the initial conditions taken from the last higher reduced velocity. In Fig. 4 solid lines represent amplitude and frequency with increasing reduced velocity and dashed lines represent amplitude and frequency with decreasing reduced velocity.

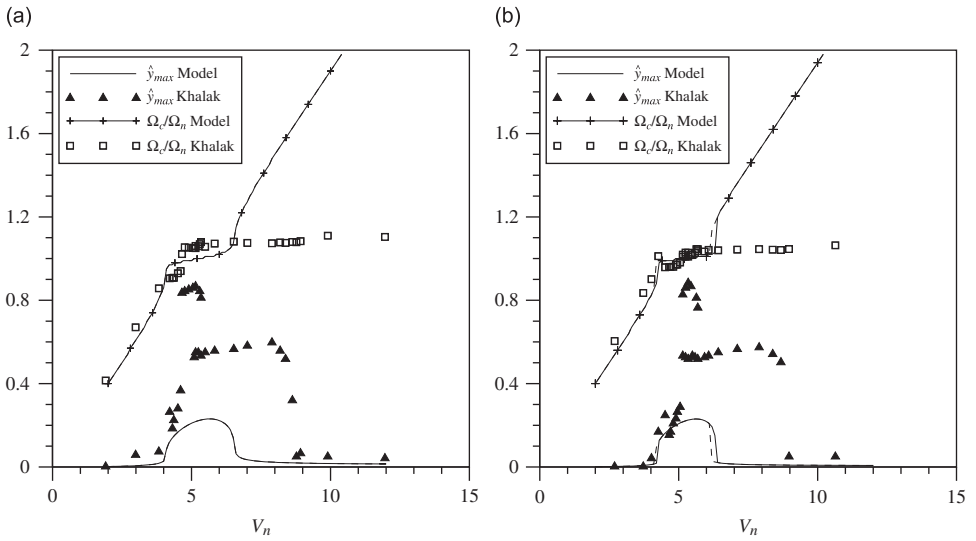

Fig. 4. Comparison of amplitude and frequency of oscillation of the model of Facchinetti et al. [35] with the measurements of Khalak et al. [11] for: (a) m^*=10.3 and (b) m^*=20.6. Solid lines represent quantities for increasing V_n, dashed lines for decreasing V_n.

From Fig. 4 it is clear that the original model of Facchinetti et al. underpredicts the amplitude of motion with a considerable margin. This can also be seen in Fig. 9 of their paper [35], in which the amplitude is plotted in a log-scale. In Fig. 4, the width of the lock-in range is underpredicted as well for both mass ratios. The model predictions are so far off from the measurements, that we therefore first start with trying to retune the original model of Facchinetti et al.

As one of the objectives of this paper is to use one model to describe both the free and forced vibration experiments of Khalak et al. and Gopalkrishnan, it seems natural to use values for $\hat{C}^0_{y1}$ and St as measured in one of these experiments. Gopalkrishnan has measured the following values, which will be used from hereon: $\hat{C}^0_{y1}=0.3842$ and St=0.1932. This leaves the variables $\hat{C}^0_{x0}$, A and ε free to tune the model with. Several runs have been made with various values for these variables. In general it can be said, that when the original wake oscillator of Facchinetti et al. is tuned to model the height of the plateau of the lower branch correctly, the width of the lock-in range is underpredicted, and that when the oscillator is tuned to correctly model the width of the lock-in range, the height of the plateau is overestimated. The problem seems to come down to the constant value of the fluid added damping in Eq. (21). This added damping, $\hat{C}^0_{x0}(\rho D^2 L)/(m+m_a)/(4\pi\,\mathrm{St})$, is too small at low reduced velocities and too large at high reduced velocities. It turns out that without the small angle assumption the model, now given by Eqs. (20) and (14), can be tuned much more easily. To stay consistent with previous assumptions, for $\hat{C}^0_{x0}$ the value measured by Gopalkrishnan will be used, that is, $\hat{C}^0_{x0}=1.1856$.

3.2.3. *Tuning of the current model to the upper and lower branches of the free vibration experiments*

As far as it has been tried in the past to tune wake oscillator models to free vibration experiments, it has implicitly been assumed that the wake oscillator should model the plateau of the lower branch of the amplitude plot. In this paper the coupling term in Eq. (14) will be made frequency dependent. When doing this, one can start with a model that describes the lower branch and then try to model the upper branch with the inclusion of frequency dependent effects, or vice versa, start with the upper branch and try to find the lower. Not knowing in advance which way to go, both will be done. The case in which the model is tuned to the upper branch will be called 'Case U' and the other case 'Case L'.

In Fig. 5 the model determined by Eqs. (20) and (14) has been tuned to the free vibration experiments of Khalak et al. The amplitude and frequency of Case U have been depicted with a bold solid line and those of Case L with a thin solid line. As before, dashed lines show amplitude and frequency for decreasing reduced velocities. Note that for Case U, the lock-in range at all mass ratios is necessarily too small. The parameters used for Cases U and L are:

$$\begin{array}{ll} \text{Case U} & \text{Case L} \\ \hat{C}^0_{x0}=1.1856, & \hat{C}^0_{x0}=1.1856, \\ \hat{C}^0_{y1}=0.3842, & \hat{C}^0_{y1}=0.3842, \\ \mathrm{St}=0.1932, & \mathrm{St}=0.1932, \\ A=4.0, & A=12.0, \\ \varepsilon=0.05, & \varepsilon=0.7. \end{array} \tag{22}$$

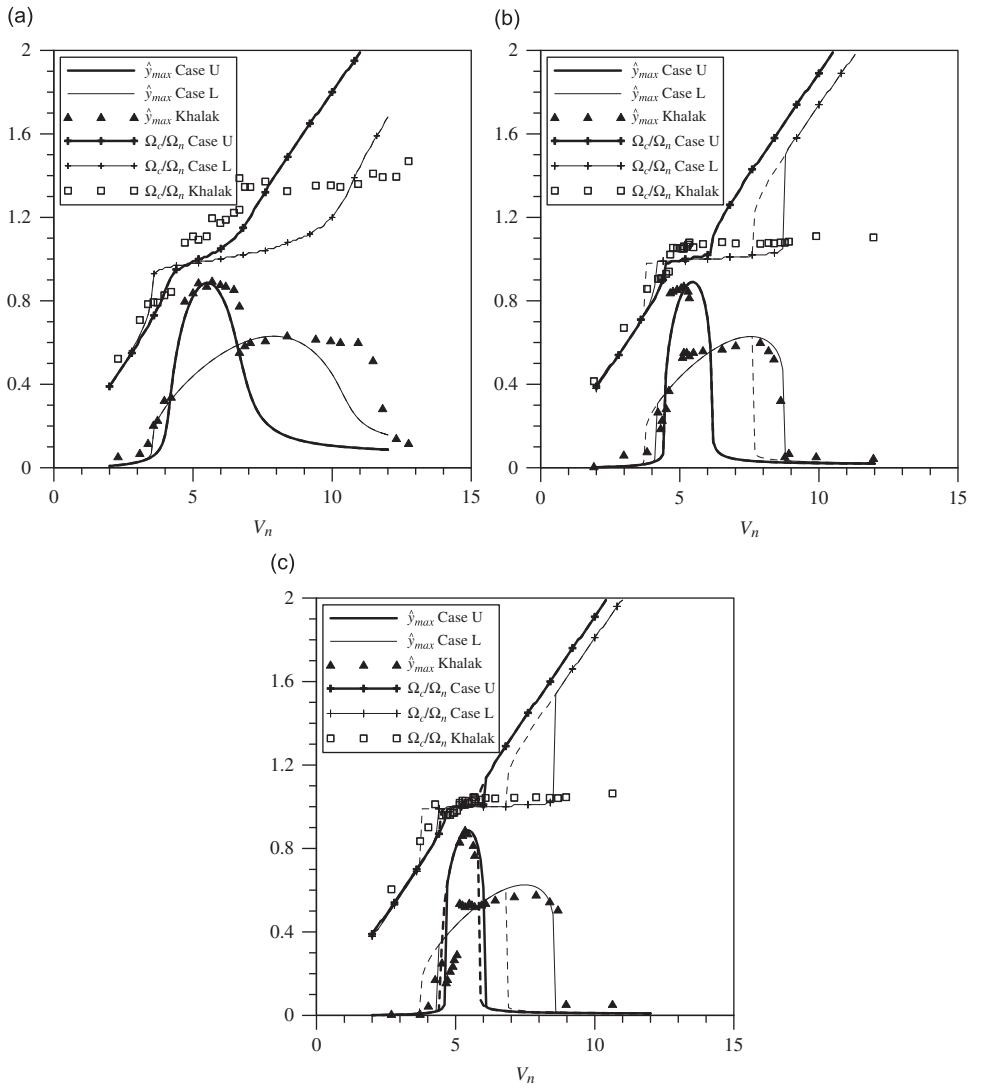

Fig. 5. Tuning of amplitude and frequency of oscillation of the adjusted model of Facchinetti et al. [35] to the measurements of Khalak et al. [11] for: (a) m^*=2.4, (b) m^*=10.3 and (c) m^*=20.6. Solid lines represent quantities for increasing V_n, dashed lines for decreasing V_n.

In most wake oscillator models it is assumed that the parameter ε is much smaller than 1. This assumption makes it possible to find solutions to the Van der Pol equation based on perturbation theory. This is however not a necessary assumption. Larger values of ε will simply result in a stronger nonlinear behavior of the Van der Pol equation and the time series of q and $\dot{q}$ will look less like those of a simple harmonic motion. In Fig. 6 the time series for q and $\dot{q}$ and the complementary phase planes are plotted, that have been obtained by solving Eq. (14) with the parameters A and ε as specified by Facchinetti et al. and as given above for Cases U and L. For the forcing on the right-hand side of Eq. (14), $y=\hat{y}\sin\Omega_c\tau$ has been substituted with $\hat{y}=0.6$ and Ω_c=1.3 so as to represent a typical point of the lower branch of free vibration. The results obtained with the parameters of Facchinetti et al. are plotted in Fig. 6a and b, with the parameters of Case U in Fig. 6c and d and with those of Case L in Fig. 6e and f. Plots 6a and 6b and 6e and 6f look very similar. Therefore the relatively high value of ε for Case L does not have to be considered as being problematic.

3.2.4. Comparison of the newly tuned model with the experimental forced vibration results

Before continuing with making the coupling term in Eq. (14) frequency dependent, the model in its current form is first compared with the forced vibration measurements of Gopalkrishnan. As explained in Section 2.2, in this experiment, the cylinder was forced to oscillate vertically in cross-flow direction with amplitude $\hat{y}$ and frequency Ω_c:

$$y(\tau)=\hat{y}\sin\Omega_c\tau. \tag{23}$$

As before, the fluid force in the vertical direction consists of a vortex force and a potential added mass force. Since the small angle assumption is not used, the model should also be able to describe the fluid forces on the cylinder in the horizontal direction. The cylinder is not being oscillated in this direction, so the potential force in this direction is zero.

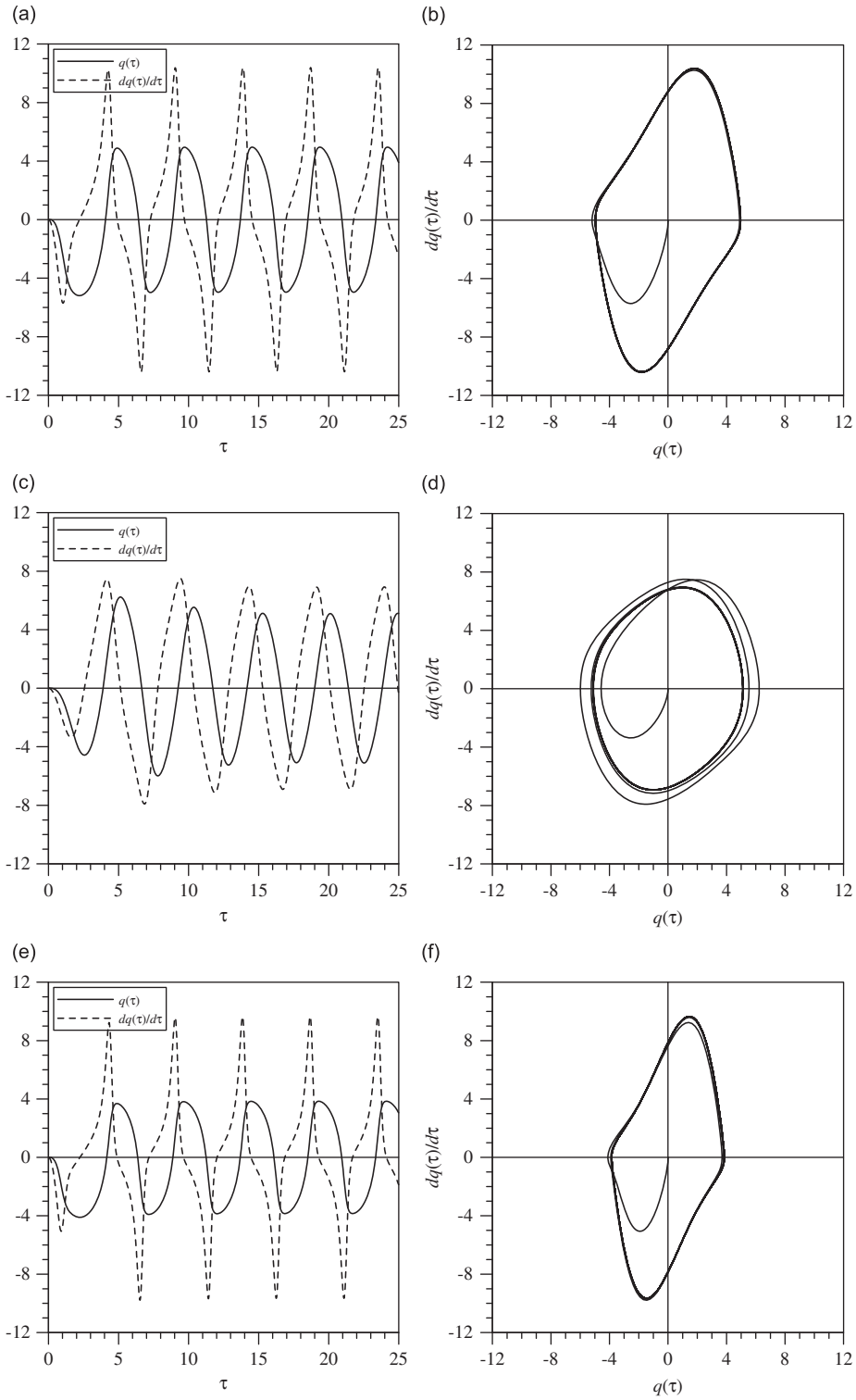

Fig. 6. Time series of the forced Van der Pol equation for q and $\dot{q}$ and the corresponding phase planes for: (a, b) $A=12.0$ and $\varepsilon=0.3$, (c, d) $A=4.0$ and $\varepsilon=0.05$ and (e, f) $A=12.0$ and $\varepsilon=0.7$.

Hence, the total horizontal and vertical fluid forces on a cylinder forced to oscillate in cross-flow direction are given by

$$F_x^y = F_{VX} = \tfrac{1}{2}\rho D V^2 L C_{VX}, \tag{24}$$

$$F_y^y = F_{VY} + F_{AY} = \frac{1}{2}\rho D V^2 L C_{VY} - \hat{C}_A \frac{\pi}{4}\rho D^2 L \frac{\mathrm{d}^2 Y}{\mathrm{d}t^2}. \tag{25}$$

Making these nondimensional results in

$$C_x^y = C_{VX}, \tag{26}$$

$$C_y^y = C_{VY} + \frac{F_{AY}}{\frac{1}{2}\rho D V^2 L} = C_{VY} - \hat{C}_A 2\pi^3\ \mathrm{St}^2\ \ddot{y}. \tag{27}$$

And the vortex forces in horizontal and vertical direction are given by

$$C_{VX} = (C_{VD}\cos\beta - C_{VL}\sin\beta)\frac{U^2}{V^2} = (C_{VD} + 2\pi\ \mathrm{St}\ \dot{y} C_{VL})\sqrt{1+4\pi^2\ \mathrm{St}^2\ \dot{y}^2}, \tag{28}$$

$$C_{VY} = (C_{VD}\sin\beta + C_{VL}\cos\beta)\frac{U^2}{V^2} = (-2\pi\ \mathrm{St}\ \dot{y} C_{VD} + C_{VL})\sqrt{1+4\pi^2\ \mathrm{St}^2\ \dot{y}^2}. \tag{16}$$

For the vortex drag and lift forces the same assumptions are made as in the free vibration modeling. As specified by Eq. (19), C_{VD} is equal to $\hat{C}_{x0}^0$ and C_{VL} is equal to $\hat{C}_{y1}^0\ q/\hat{q}_1$. The variable q is now given by the uncoupled wake oscillator, in which Eq. (23) is substituted on the right hand side:

$$\ddot{q} + \varepsilon(q^2-1)\dot{q} + q = -A\Omega_c^2 \hat{y}\sin\Omega_c\tau \tag{29}$$

The forced vibration is modeled by solving the forced oscillator given by Eq. (29). Then, the vortex forces in horizontal and vertical direction can be found with Eqs. (16), (19) and (28) and the total fluid forces are given by Eqs. (26) and (27). In the preceding equations the derivatives of y can be calculated using Eq. (23). The force coefficients $\hat{C}_{y1a}^y$, $\hat{C}_{y1v}^y$ and $\hat{C}_{x0}^y$ are found as

$$\hat{C}_{y1a}^y = \frac{2}{\mathcal{T}_c}\int_{\tau_0}^{\tau_0+\mathcal{T}_c} C_y^y \sin(\Omega_c\tau)\,\mathrm{d}\tau = \frac{2}{\mathcal{T}_c}\int_{\tau_0}^{\tau_0+\mathcal{T}_c} C_{VY}\sin(\Omega_c\tau)\,\mathrm{d}\tau + \hat{C}_A 2\pi^3\ \mathrm{St}^2\ {\Omega_c}^2\hat{y}, \tag{30}$$

$$\hat{C}_{y1v}^y = -\frac{2}{\mathcal{T}_c}\int_{\tau_0}^{\tau_0+\mathcal{T}_c} C_y^y \cos(\Omega_c\tau)\,\mathrm{d}\tau = -\frac{2}{\mathcal{T}_c}\int_{\tau_0}^{\tau_0+\mathcal{T}_c} C_{VY}\cos(\Omega_c\tau)\,\mathrm{d}\tau, \tag{31}$$

$$\hat{C}_{x0}^y = \frac{1}{\mathcal{T}_c}\int_{\tau_0}^{\tau_0+\mathcal{T}_c} C_x^y\,\mathrm{d}\tau = \frac{1}{\mathcal{T}_c}\int_{\tau_0}^{\tau_0+\mathcal{T}_c} C_{VX}\,\mathrm{d}\tau. \tag{32}$$

Similar to the free vibration calculations, Eq. (29) has been solved numerically in the time domain at a certain reduced velocity V_c. The first 50 periods of the time series of C_y^y and C_x^y have been disregarded and the force coefficients have been determined by averaging over the next 50 periods. The coefficients have been determined in the range V_c=3–12 with a stepsize of dV_c=0.01. The initial conditions that have been used for all calculation are $q(0)=0.01$ and $\dot{q}(0)=0$.

The results of the forced vibration calculations for Cases U and L are plotted in Fig. 7. Solid lines represent the measurements of Gopalkrishnan and dashed lines the results of the wake oscillator. The dashed lines are labeled with the amplitude for which they have been obtained. Although the results of the oscillator are far from exact, the major trends in the data seem to be modeled surprisingly well. In Fig. 7a and b, the substantial increase of $\hat{C}_{y1a}^y$ at low V_c is caused by the potential added mass term $\hat{C}_A 2\pi^3\ \mathrm{St}^2\ {\Omega_c}^2\hat{y} = \hat{C}_A 2\pi^3\hat{y}/V_c$. At high V_c the measurements show negative values for $\hat{C}_{y1a}^y$, while those of the model are positive. Although the part of the modeled fluid force given by the wake oscillator returns negative values, it is the addition of the positive added mass force that results in a positive total force at high V_c. In Fig. 7c and d, the model finds both for Cases U and L, high positive values for $\hat{C}_{y1v}^y$ at low V_c, then, just as in the measurements, negative values at low amplitudes and subsequently the model finds low positive values for all amplitudes at high V_c. The positive values at low V_c can only be modeled by correctly accounting for the angle β in Eq. (16), as they are mainly caused by the part of $-2\pi\ \mathrm{St}\ \dot{y} C_{VD}\sqrt{1+4\pi^2\ \mathrm{St}^2\ \dot{y}^2}$ that is in phase with the cylinder velocity. The most surprising result of fully accounting for the angle β is however the capability of the model to describe the increased average horizontal in-line force on an oscillating cylinder. As can be seen in Fig. 7e and f, the order of magnification of $\hat{C}_{x0}^y$ is predicted fairly well.

Although it may seem surprising that the major trends in the measurements of Gopalkrishnan can be reproduced with the current oscillator model, a closer inspection reveals that by removing the small angle assumption, the cross-flow fluid

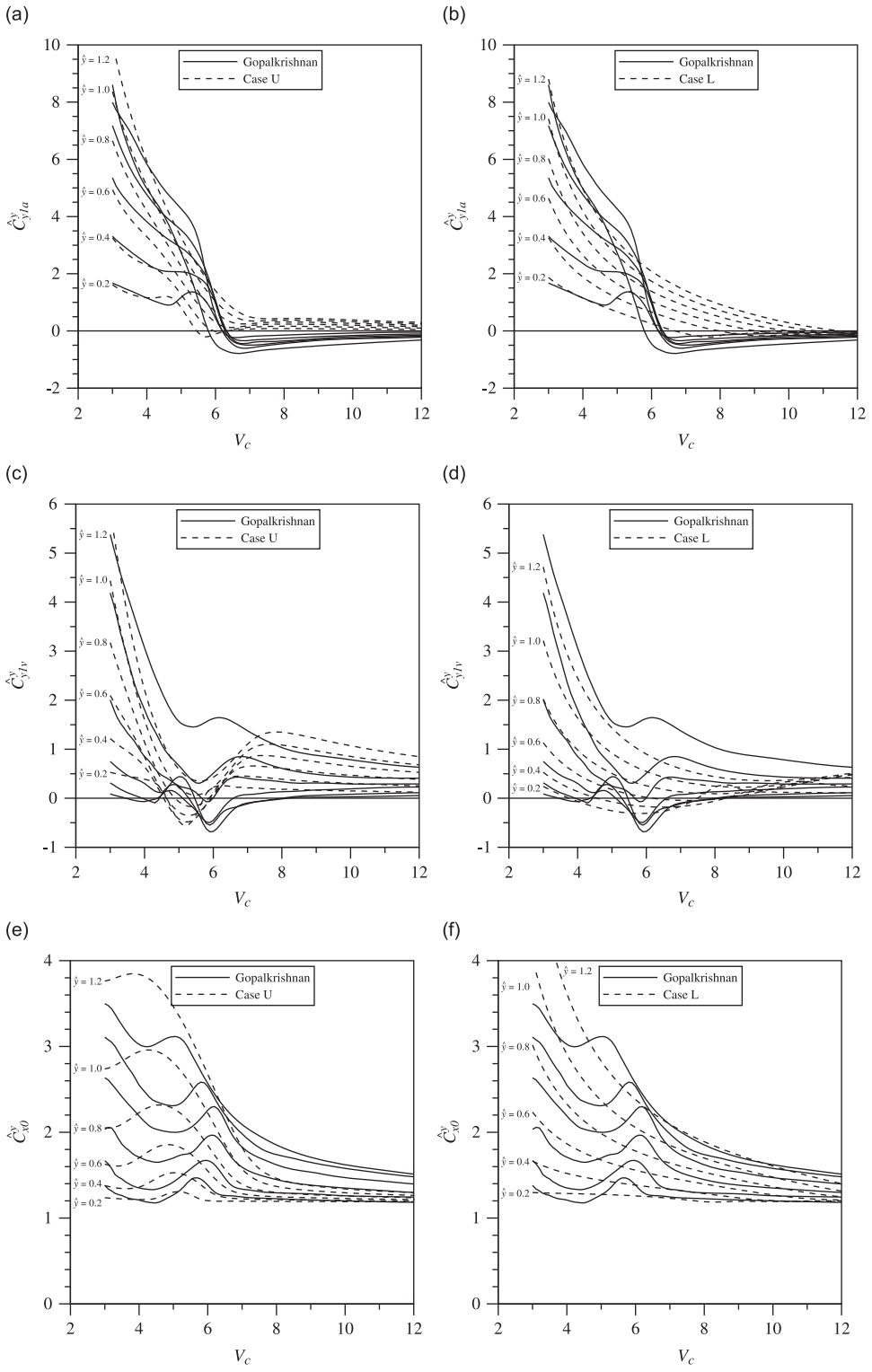

Fig. 7. Comparison of the adjusted model of Facchinetti et al. [35] with the measurements of Gopalkrishnan [10] for: (a, b) the force coefficient $\hat{C}^y_{y1a}$, (c, d) the force coefficient $\hat{C}^y_{y1v}$ and (e, f) the force coefficient $\hat{C}^y_{x0}$.

force F^y_y is very similar to the fluid force predicted by the Morison equation [38]. The Morison equation is known to give acceptable results over a range of Keulegan–Carpenter numbers for a cylinder oscillating with respect to the surrounding fluid. In the limiting case, when V=0, F^y_y is even equal to the force predicted by the Morison equation. In dimensional form

F_y^y is given by the following equation (see Eqs. (8), (9) and (25)):

$$F_y^y = \frac{1}{2}\rho D V^2 L C_{VY} - \hat{C}_A \frac{\pi}{4}\rho D^2 L \frac{\mathrm{d}^2 Y}{\mathrm{d}t^2}$$
$$= \frac{1}{2}\rho D L\left(-C_{VD}\frac{\mathrm{d}Y}{\mathrm{d}t} + C_{VL}V\right)\sqrt{V^2 + \left(\frac{\mathrm{d}Y}{\mathrm{d}t}\right)^2} - \hat{C}_A \frac{\pi}{4}\rho D^2 L \frac{\mathrm{d}^2 Y}{\mathrm{d}t^2}.$$

Setting $V=0$ in the above equation results in

$$F_y^y = -\left(\frac{1}{2}\rho D L C_{VD}\frac{\mathrm{d}Y}{\mathrm{d}t}\left|\frac{\mathrm{d}Y}{\mathrm{d}t}\right| + \hat{C}_A \frac{\pi}{4}\rho D^2 L \frac{\mathrm{d}^2 Y}{\mathrm{d}t^2}\right), \tag{33}$$

which is exactly the Morison equation.

4. Derivation of frequency dependent coupling

Instead of using one value for the coupling coefficient A for all reduced velocities, the wake oscillator model that is presented in the preceding section, could be improved by tuning the coupling coefficient for each reduced velocity separately. This would make the coupling coefficient a function of the reduced velocity or its reciprocal, the frequency of cylinder motion. This frequency dependent behavior is represented in the time domain by a convolution integral. In this specific case, this integral should contain a kernel that is convoluted with the cylinder displacement or its derivatives. This kernel can be found from the frequency dependent coupling coefficient $A(\Omega)$ using an appropriate integral transform. In this manner the free vibration can be modeled including frequency dependent coupling effects and without an assumption of a dominant frequency, provided that $A(\Omega)$ is known in the frequency domain. The coefficient $A(\Omega)$ can be found by tuning the wake oscillator per frequency to the results of the forced vibration measurements. This will be done in the next section. Before that, however, it is necessary to find the correct integral relation between the frequency dependent coefficient and the convolution kernel.

Facchinetti et al. [35] have shown that the acceleration coupling gives the best description of the cylinder forcing on the Van der Pol equation. This does not necessarily imply that a velocity coupling cannot be present. The acceleration coupling is merely dominant. The derivation therefore starts with a coupling in phase with the cylinder acceleration and one in phase with the cylinder velocity. An additional displacement coupling is not necessary as it is in anti-phase with the acceleration coupling. So the steady state harmonic motion of the forced wake oscillator is now given by

$$\ddot{q} + \varepsilon(q^2-1)\dot{q} + q = \tilde{A}(\Omega)\ddot{y} + \tilde{B}(\Omega)\dot{y}, \tag{34}$$

where $\tilde{A}(\Omega)$ and $\tilde{B}(\Omega)$ are the acceleration and velocity coupling coefficients that are functions of the frequency Ω. Note that as all frequencies in this section will be the actual frequency of cylinder oscillation, the subscript in the notation of the frequency is dropped. To describe the free vibration the right-hand side of the above equation should be replaced by convolution integrals:

$$\ddot{q} + \varepsilon(q^2-1)\dot{q} + q = \int_{-\infty}^{\tau} K_A(\tau-\tilde{\tau})\ddot{y}(\tilde{\tau})\,\mathrm{d}\tilde{\tau} + \int_{-\infty}^{\tau} K_B(\tau-\tilde{\tau})\dot{y}(\tilde{\tau})\,\mathrm{d}\tilde{\tau}, \tag{35}$$

in which K_A denotes the kernel that is convoluted with the cylinder acceleration and K_B the kernel that is convoluted with the velocity. Both convolution kernels are restricted by two constraints. The first ascertains that the memory effects that are contained in the kernel die out over long enough time and that the convolution integral converges. It is given by

$$\lim_{\tau\to\infty} K(\tau) = 0 \tag{36}$$

The second constraint is a causality condition. The cylinder cannot force the wake before it is oscillating itself. This can be enforced by changing the integration limits in Eq. (35) from $-\infty$ to 0:

$$\ddot{q} + \varepsilon(q^2-1)\dot{q} + q = \int_{0}^{\tau} K_A(\tau-\tilde{\tau})\ddot{y}(\tilde{\tau})\,\mathrm{d}\tilde{\tau} + \int_{0}^{\tau} K_B(\tau-\tilde{\tau})\dot{y}(\tilde{\tau})\,\mathrm{d}\tilde{\tau}. \tag{37}$$

When a steady state is reached, Eqs. (34) and (37) should give the same results. This can be expressed as

$$\tilde{A}(\Omega)\ddot{y} + \tilde{B}(\Omega)\dot{y} = \lim_{\tau\to\infty}\left(\int_0^{\tau} K_A(\tau-\tilde{\tau})\ddot{y}(\tilde{\tau})\,\mathrm{d}\tilde{\tau} + \int_0^{\tau} K_B(\tau-\tilde{\tau})\dot{y}(\tilde{\tau})\,\mathrm{d}\tilde{\tau}\right)$$
$$= \int_0^{\infty} K_A(\tau-\tilde{\tau})\ddot{y}(\tilde{\tau})\,\mathrm{d}\tilde{\tau} + \int_0^{\infty} K_B(\tau-\tilde{\tau})\dot{y}(\tilde{\tau})\,\mathrm{d}\tilde{\tau}$$
$$= \int_0^{\infty} K_A(\tilde{\tau})\ddot{y}(\tau-\tilde{\tau})\,\mathrm{d}\tilde{\tau} + \int_0^{\infty} K_B(\tilde{\tau})\dot{y}(\tau-\tilde{\tau})\,\mathrm{d}\tilde{\tau}. \tag{38}$$

Substitution of the cylinder motion, $y(\tau) = \hat{y}\sin(\Omega\tau)$, into the above expression results in

$$-\Omega^2\hat{y}\tilde{A}\sin(\Omega\tau) + \Omega\hat{y}\tilde{B}\cos(\Omega\tau)$$

$$= -\Omega^2\hat{y}\left(\sin(\Omega\tau)\int_0^\infty K_A(\tilde{\tau})\cos(\Omega\tilde{\tau})\,\mathrm{d}\tilde{\tau} - \cos(\Omega\tau)\int_0^\infty K_A(\tilde{\tau})\sin(\Omega\tilde{\tau})\,\mathrm{d}\tilde{\tau}\right)$$
$$+\Omega\hat{y}\left(\cos(\Omega\tau)\int_0^\infty K_B(\tilde{\tau})\cos(\Omega\tilde{\tau})\,\mathrm{d}\tilde{\tau} + \sin(\Omega\tau)\int_0^\infty K_B(\tilde{\tau})\sin(\Omega\tilde{\tau})\,\mathrm{d}\tilde{\tau}\right). \quad (39)$$

Collection of terms multiplied by $\sin(\Omega\tau)$ and $\cos(\Omega\tau)$ provides the integral relations between $\tilde{A}(\Omega)$, $\tilde{B}(\Omega)$, $K_A(\tau)$ and $K_B(\tau)$:

$$\tilde{A}(\Omega) = \int_0^\infty K_A(\tau)\cos(\Omega\tau)\,\mathrm{d}\tau - \frac{1}{\Omega}\int_0^\infty K_B(\tau)\sin(\Omega\tau)\,\mathrm{d}\tau,$$
$$\tilde{B}(\Omega) = \Omega\int_0^\infty K_A(\tau)\sin(\Omega\tau)\,\mathrm{d}\tau + \int_0^\infty K_B(\tau)\cos(\Omega\tau)\,\mathrm{d}\tau. \quad (40)$$

The above relations show that *both* convolution integrals in Eq. (37) result in a forcing on the wake oscillator that contains a part in phase with the cylinder acceleration as well as a part in phase with the cylinder velocity. Therefore, one of the convolution integrals is redundant and can be dropped. It seems natural to drop the integral containing the cylinder velocity, to keep the appearance of an acceleration coupling, but for practical reasons that will become clear in Section 5, it is most convenient to convolute a kernel with the lowest derivative of y. The first integral is therefore dropped and the second one retained. Hence: $K_A(\tau)=0$, and the remaining variables are redefined as follows:

$$K(\tau) = K_B(\tau), \quad (41)$$

$$A(\Omega) = \Omega\tilde{A}(\Omega) = -\int_0^\infty K(\tau)\sin(\Omega\tau)\,\mathrm{d}\tau, \quad (42)$$

$$B(\Omega) = \tilde{B}(\Omega) = \int_0^\infty K(\tau)\cos(\Omega\tau)\,\mathrm{d}\tau. \quad (43)$$

Eqs. (42) and (43) reveal that with this specific definition the frequency dependent coefficients, $A(\Omega)$ and $B(\Omega)$, are in fact the imaginary and real parts of the Laplace transform, as given in Eq. (44), provided that the Laplace constant s in this transform is defined as being purely imaginary: $s=\mathrm{i}\Omega$:

$$F(s) = \mathcal{L}\{f(\tau)\} = \int_0^\infty \mathrm{e}^{-s\tau}f(\tau)\,\mathrm{d}\tau. \quad (44)$$

And therefore:

$$B(\Omega) = \mathrm{Re}(\mathcal{L}\{K(\tau)\}|_{s=\mathrm{i}\Omega}),\ A(\Omega) = \mathrm{Im}(\mathcal{L}\{K(\tau)\}|_{s=\mathrm{i}\Omega}). \quad (45)$$

So it is found that the convolution kernel $K(\tau)$ is simply the inverse Laplace transform of $B(\Omega)+\mathrm{i}A(\Omega)$:

$$K(\tau) = \mathcal{L}^{-1}\{B(\Omega)+\mathrm{i}A(\Omega)|_{\Omega=-\mathrm{i}s}\}. \quad (46)$$

Summarizing, to improve the wake oscillator without having to make an assumption of a dominant frequency of motion, the term $A(\Omega)\ddot{y}/\Omega+B(\Omega)\dot{y}$ is replaced by $\int_0^\tau K(\tau-\tilde{\tau})\dot{y}(\tilde{\tau})\,\mathrm{d}\tilde{\tau}$ under the condition that for large enough τ the two terms return the same steady state forcing and it is found that the relation between the convolution kernel and the frequency dependent coefficients is then given by Eq. (46).

It is interesting to note in Eqs. (42), (43) and (45) that the frequency dependent coefficients $A(\Omega)$ and $B(\Omega)$ are not independent of each other, as they are the imaginary and real parts of the same transform and are contained in one and the same convolution kernel. If the inverse Fourier sine and cosine transforms are taken from Eqs. (42) and (43), the following expressions are obtained:

$$K(\tau) = -\frac{2}{\pi}\int_0^\infty \left(A(\Omega) - \Omega\lim_{\tilde{\Omega}\to\infty}\left(A(\tilde{\Omega})/\tilde{\Omega}\right)\right)\sin(\Omega\tau)\,\mathrm{d}\Omega$$
$$= \frac{2}{\pi}\int_0^\infty (B(\Omega)-B(0))\cos(\Omega\tau)\,\mathrm{d}\Omega, \quad (47)$$

where attention has been paid to correctly incorporate the conditions at $\Omega=0$ and $\Omega=\infty$. The above expressions show that the convolution kernel can in fact be determined from $A(\Omega)$ or $B(\Omega)$ alone, under the condition that $A(\Omega)$ or $B(\Omega)$ is known over the entire frequency range from $\Omega=0$ to $\Omega=\infty$. This implies as well that if one of the coefficients is known over the entire frequency range, the other one is completely determined except for a constant in the case of $B(\Omega)$ and a constant multiplied by Ω in the case of $A(\Omega)$. From Eq. (47) the relation between $A(\Omega)$ and $B(\Omega)$ can be expressed as

$$\int_0^\infty \left(A(\Omega) - \Omega\lim_{\tilde{\Omega}\to\infty}\left(A(\tilde{\Omega})/\tilde{\Omega}\right)\right)\sin(\Omega\tau)\,\mathrm{d}\Omega + \int_0^\infty (B(\Omega)-B(0))\cos(\Omega\tau)\,\mathrm{d}\Omega = 0. \quad (48)$$

Eq. (48) is more commonly expressed in a form in which the integral for either the left or right hand side is eliminated. The expressions that are then obtained are known as the Kramers–Kronig relations. In this specific case they are given by

$$\frac{A(\Omega)}{\Omega} - \lim_{\Omega\to\infty}\frac{A(\Omega)}{\Omega} = \frac{1}{\Omega}\frac{2}{\pi}\int_0^\infty \frac{(B(\tilde{\Omega})-B(\Omega))\Omega}{\tilde{\Omega}^2-\Omega^2}\,\mathrm{d}\tilde{\Omega}, \quad (49)$$

$$B(\Omega)-B(0)=-\frac{2\Omega^2}{\pi}\int_0^{\infty}\frac{A(\tilde{\Omega})/\tilde{\Omega}-A(\Omega)/\Omega}{\tilde{\Omega}^2-\Omega^2}\,\mathrm{d}\tilde{\Omega}. \tag{50}$$

Derivations of the Kramers–Kronig relations can be found in the books by Elmore and Head [39] and De Hoop [40]. The Kramers–Kronig relations give the relationship between the in-phase and out-of-phase part of the response of a causal linear system and although the wake oscillator is a nonlinear equation, the Kramers–Kronig relations are encountered here, because the coupling term is linear and causal.

5. Application of frequency dependent coupling

5.1. Determination of the coefficients A and B as functions of the frequency of oscillation

Eq. (46) shows that the time domain convolution kernel K can be found as the inverse Laplace transform of the frequency domain coefficients A and B. Therefore, it is first needed to determine A and B in the frequency domain. As the forced vibration experiments are essentially carried out in the frequency domain, this provides the opportunity to use these experiments to determine A and B. This is done by using the wake oscillator to model the forced vibration. Then, by changing A and B in the model an error function is minimized that characterizes the discrepancy between the model predictions and the measurements of Gopalkrishnan.

Firstly, the coupling term as determined in the previous section is applied to the right-hand side of the oscillator equation:

$$\ddot{q}+\varepsilon(q^2-1)\dot{q}+q=A/\Omega_c\ddot{y}+B\dot{y},\quad \text{substitution of}:\ \ y(\tau)=\hat{y}\sin(\Omega_c\tau),$$

results in

$$\ddot{q}+\varepsilon(q^2-1)\dot{q}+q=-\Omega_c A\hat{y}\sin(\Omega_c\tau)+\Omega_c B\hat{y}\cos(\Omega_c\tau). \tag{51}$$

This equation has been solved numerically in the same manner as before with the value for ε and the initial values for A and B equal to the values given by (22). That is, the initial value for B is zero and the initial value for A has been adjusted because of the multiplication with Ω_c in Eq. (42). Then, the fluid force coefficients $\hat{C}^y_{y1a}$, $\hat{C}^y_{y1v}$ and $\hat{C}^y_{x0}$ have been calculated with Eqs. (30), (31) and (32). When these values are known, the error can be determined. The error has initially been defined on the basis of $\hat{C}^y_{y1a}$ and $\hat{C}^y_{y1v}$, as the values of these coefficients could be read most accurately from [10,13]:

$$\text{error}=(\hat{C}^y_{y1a;\text{model}}-\hat{C}^y_{y1a;\text{measured}})^2+(\hat{C}^y_{y1v;\text{model}}-\hat{C}^y_{y1v;\text{measured}})^2. \tag{52}$$

Subsequently, the error is minimized with a one-dimensional procedure that brackets the minimum and then performs a golden section search to find this minimum. This procedure is explained in detail by Press et al. in [41]. The procedure starts with changing A and keeping B constant and when under these conditions a minimum has been found, A is kept constant and B is changed. This is repeated over and over again until the error given by (52) is smaller than a preset value. The procedure is quite time consuming, as every single evaluation of (52) involves solving Eq. (51) for 100 periods and then performing an integration over the time series to determine the fluid force coefficients.

It is essential to understand that the measurements of Gopalkrishnan have been conducted at several amplitudes of forced vibration and that at every amplitude different fluid forces have been measured. But when modeling the free vibration with the wake oscillator containing the convolution integral, one kernel K based on one set of frequency dependent curves $A(\Omega_c)$ and $B(\Omega_c)$ should be able to describe the fluid force behavior for all amplitudes of cylinder motion. The minimization procedure should therefore find the same set of curves for $A(\Omega_c)$ and $B(\Omega_c)$, regardless of the amplitude at which the forced vibration measurements, that have been used to determine $A(\Omega_c)$ and $B(\Omega_c)$, have been conducted. This is a 'check of correctness' of the model. If the model contains the right nonlinearities, the right coupling and the right tuning, one set of frequency dependent parameters should be able to describe the behavior of the fluid forces at all amplitudes of motion.

Starting at V_c=3 (with Ω_c=1/St/V_c) and $\hat{y}$=0.2 the error is minimized until it is smaller than 10^{-6}. Then at the same amplitude the reduced velocity V_c is increased with dV_c=0.1 and the calculations are repeated until the whole frequency range at this amplitude is covered, each time using the final A and B at the previous frequency as the initial values for the iterative procedure at the next frequency. In this manner the frequency dependent parameters $A(\Omega_c)$ and $B(\Omega_c)$ have been determined for the amplitudes of forced motion in the range of $\hat{y}=0.2-1.2$ with a stepsize of $d\hat{y}=0.1$.

The resulting curves for A and B for 6 amplitudes of forced vibration are plotted in Fig. 8a and b for Case U and in Fig. 8c and d for Case L. It is clear from these figures that in both cases different curves for A and B are found at different amplitudes of forcing, implying that with the current model the results of Gopalkrishnan cannot be reproduced with a single set of frequency dependent parameters. It appears that the wake oscillator as tuned in Case U gives better results than as tuned in Case L, since in Fig. 8a and b the spread in the curves of A and B for different amplitudes is one order of magnitude smaller than in Fig. 8c and d.

It has been attempted to reduce the spread in the curves of A and B in a number of ways, while keeping the simplicity of the original model intact. First of all, the error has been redefined by including the horizontal fluid force coefficient $\hat{C}^y_{x0}$,

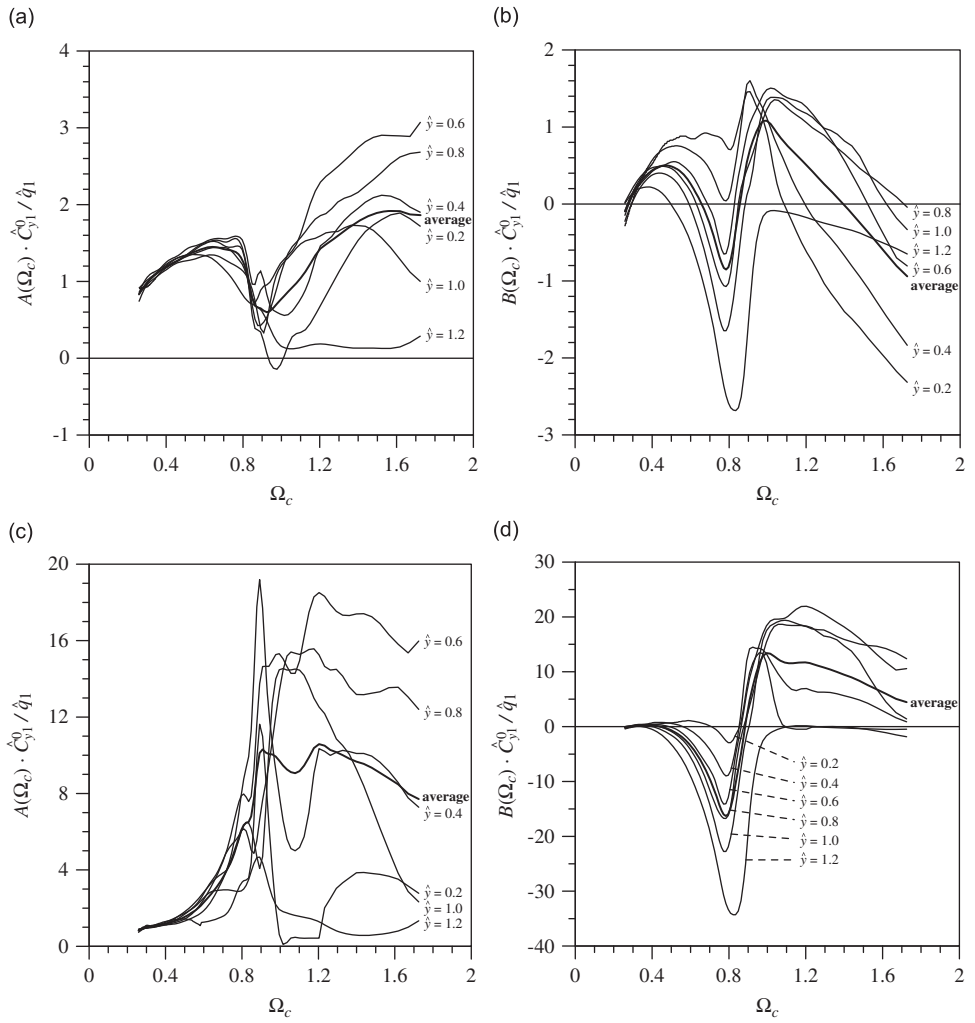

Fig. 8. Curves found through a minimization procedure for: (a) the coefficient A for Case U, (b) the coefficient B for Case U, (c) the coefficient A for Case L and (d) the coefficient B for Case L.

giving

$$\text{error} = (\hat{C}^y_{y1a;\text{model}} - \hat{C}^y_{y1a;\text{measured}})^2 + (\hat{C}^y_{y1v;\text{model}} - \hat{C}^y_{y1v;\text{measured}})^2 + (\hat{C}^y_{x0;\text{model}} - \hat{C}^y_{x0;\text{measured}})^2.$$

Except for increasing the number of iterations and making it impossible to satisfy a small error requirement around $\Omega_c = 1$, this did not have a noticeable effect on the spread of the curves of A and B. Secondly, it has been tried to retune the model by changing the value of the parameters given by (22). Special attention has been given to the parameter ε which multiplies the nonlinearity. In general it can be said that lower values of ε give less spread in the curves of A and B, but no value has been found that reduces the spread considerably compared to the spread in the curves as found in Case U. Finally, the Van der Pol equation has been replaced with the Rayleigh equation to see whether that would improve matters. Eq. (51) is then replaced by

$$\ddot{q} + \varepsilon(\dot{q}^2 - 1)\dot{q} + q = -\Omega_c A\hat{y}\sin(\Omega_c\tau) + \Omega_c B\hat{y}\cos(\Omega_c\tau). \tag{53}$$

The amplitude of the limit cycle of the Rayleigh equation is $\hat{q}_1 = 2/\sqrt{3}$. As before, the Rayleigh equation is first tuned to the upper branch ($\varepsilon = 0.05$; $A = 2.0$) and lower branch ($\varepsilon = 1.0$; $A = 6.5$) of the free vibration plot and then for both cases the curves for $A(\Omega_c)$ and $B(\Omega_c)$ have been determined with the minimization procedure. The resulting curves for A and B are similar to those of Fig. 8 and still contain a relatively large spread for different amplitudes of forced vibration.

Hence, starting with the wake oscillator model of Facchinetti et al., which after retuning is already able to describe the most important features of free and forced vibration VIV and then incorporating frequency dependent coupling parameters, it is found that this model still cannot model forced vibration experiments at all amplitudes with *one* set of frequency dependent coefficients. This implies that the current model still contains one or more components that need to

be improved. The following points come to mind for possible improvement:

1. Nonlinear coupling term. It has been assumed that the acceleration coupling on the right-hand side of the wake oscillator is a linear term. Considering, that by using a nonlinear description for the vortex force C_{VY} on the right-hand side of the structural oscillator the model is improved noticeably, it could be examined whether the coupling term on the right-hand side of the wake oscillator should be dependent on the angle β as well.
2. Nonlinearity in the wake oscillator. The nonlinearity in the wake oscillator is not derived from first principles. The use of the Van der Pol or Rayleigh equation is merely an assumption. Other nonlinear oscillators that contain a limit cycle could possibly give a better description of the wake behavior and fluid forces.
3. Double wake oscillator. When looking at Fig. 5, in which the results of a wake oscillator tuned to the upper branch and one tuned to the lower branch are depicted in a single figure, one almost immediately wonders whether it would be possible to devise a model that combines two wake oscillators to describe the oscillating hydrodynamic forces. This could be justified by distinguishing two separate oscillatory processes in the wake. One could imagine the near and far wake to separately influence the fluid behavior or, for example, the boundary layer and the wake to have distinct influences on the fluid forces.

Although it proved not possible with the current oscillator model to find one set of frequency dependent coefficients based on the forced vibration experiments at different amplitudes of vibration, it is still possible that introduction of the convolution integral into the wake oscillator will improve the model predictions. It seems therefore reasonable to determine a convolution kernel K on the basis of one of the sets of curves that have been found for the frequency dependent parameters A and B.

5.2. Determination of the kernel K on the basis of the frequency dependent parameters A and B and application of the convolution integral formulation

A number of curves for A and B have been determined in the previous paragraph, but only one set of curves can be used for determining K. For that reason we start with trying to determine K on the basis of the 'average curves' for A and B. These curves are determined by averaging at every frequency over the values of A and B at the eleven amplitudes of forced vibration ($\hat{y}=0.2$, $\hat{y}=0.3$, etc. to $\hat{y}=1.2$), at which the calculations have been performed, see Fig. 8.

As explained in Section 4, the convolution kernel $K(\tau)$ is given by the inverse Laplace transform of $B(\Omega_c)+\mathrm{i}A(\Omega_c)$. However, to perform the inverse transform the frequency dependent coefficients $A(\Omega_c)$ and $B(\Omega_c)$ need to be extended over the right half-plane of the complex s-plane. A straightforward manner to extend the spectrum of A and B is with complex curve fitting. The basics of this method are explained in the papers by Levy [42] and Sanathanan and Koerner [43]. The most general form to approximate frequency domain responses is however the method of Gustavsen and Semlyen [44]. As the inverse Laplace transform of their approximation results in a convenient convolution kernel, their method will be used. The complex function to approximate is given by

$$F(s)=(B(\Omega_c)+\mathrm{i}A(\Omega_c))\big|_{\Omega_c=-\mathrm{i}s}. \tag{54}$$

Gustavsen and Semlyen approximate $F(s)$ with

$$F(s)=\sum_{m=1}^{M}\left(\frac{c_m}{s-a_m}\right)+d+sh,$$

where d and h are real and the residues c_m and poles a_m are either real or appear in complex conjugate pairs. If the second option is chosen, this gives

$$F(s)=\sum_{n=1}^{N}\left(\frac{c_n}{s-a_n}+\frac{\bar{c}_n}{s-\bar{a}_n}\right)+d+sh. \tag{55}$$

By taking the inverse Laplace transform of (55) the convolution kernel is found to be

$$K(\tau)=\mathcal{L}^{-1}\{F(s)\}=\sum_{n=1}^{N}[2\exp(a_n^{\mathrm{re}}\tau)(c_n^{\mathrm{re}}\cos(a_n^{\mathrm{im}}\tau)-c_n^{\mathrm{im}}\sin(a_n^{\mathrm{im}}\tau))]+d\delta(\tau)+h\frac{\mathrm{d}}{\mathrm{d}\tau}\delta(\tau), \tag{56}$$

in which δ denotes the Dirac delta function and the superscripts 're' and 'im' denote the real and imaginary parts of c and a. Note that to comply with constraint (36), the poles should lie in the left half-plane of the complex s-plane. Performing the convolution of the kernel and the cylinder velocity results in

$$\int_0^{\tau}K(\tau-\tilde{\tau})\dot{y}(\tilde{\tau})\,\mathrm{d}\tilde{\tau}=\int_0^{\tau}K^{*}(\tau-\tilde{\tau})\dot{y}(\tilde{\tau})\,\mathrm{d}\tilde{\tau}+d\dot{y}+h\ddot{y}, \tag{57}$$

where K^* is given by

$$K^{*}(\tau)=\sum_{n=1}^{N}[2\exp(a_n^{\mathrm{re}}\tau)(c_n^{\mathrm{re}}\cos(a_n^{\mathrm{im}}\tau)-c_n^{\mathrm{im}}\sin(a_n^{\mathrm{im}}\tau))]. \tag{58}$$

The reason for choosing in Section 4 to convolute the kernel K with $\dot{y}$ instead of with $\ddot{y}$ is that in the most general approximation for K the derivative of the Dirac delta appears. Convolution of K with the acceleration $\ddot{y}$ would have resulted in a term dependent on $\ddot{y}$.

The method of Gustavsen and Semlyen consists of finding an approximation for $F(s)$ by guessing a set of initial poles a_n and multiplying $F(s)$ with a scaling function. The resulting augmented system is linear and can be solved with a least squares method. On the basis of the solution of the augmented system an improved set of poles a_n can be found and again the resulting linear system can be solved with a least squares method, so that the residues c_n and the values of d and h are found. The starting poles can influence the final results of the procedure. For the initial guess of the poles Gustavsen and Semlyen advise a negative real part and imaginary parts that are linearly distributed over the frequency range of interest. Further details on the procedure are given in their paper [44].

In general it can be said that this method works very well. If frequency dependent curves were constructed based on a set of poles (with negative real parts), residues and values of d and h, it proved always possible to recover the poles, residues and d and h with this procedure on the basis of the curves as long as the order N was the same as the order that had been used to construct the curves. This even worked if poor initial guesses for the starting poles were used. If an order N was used that was slightly higher than the order used to construct the curves, the original poles and residues were found plus additional poles, of which the residues were negligible.

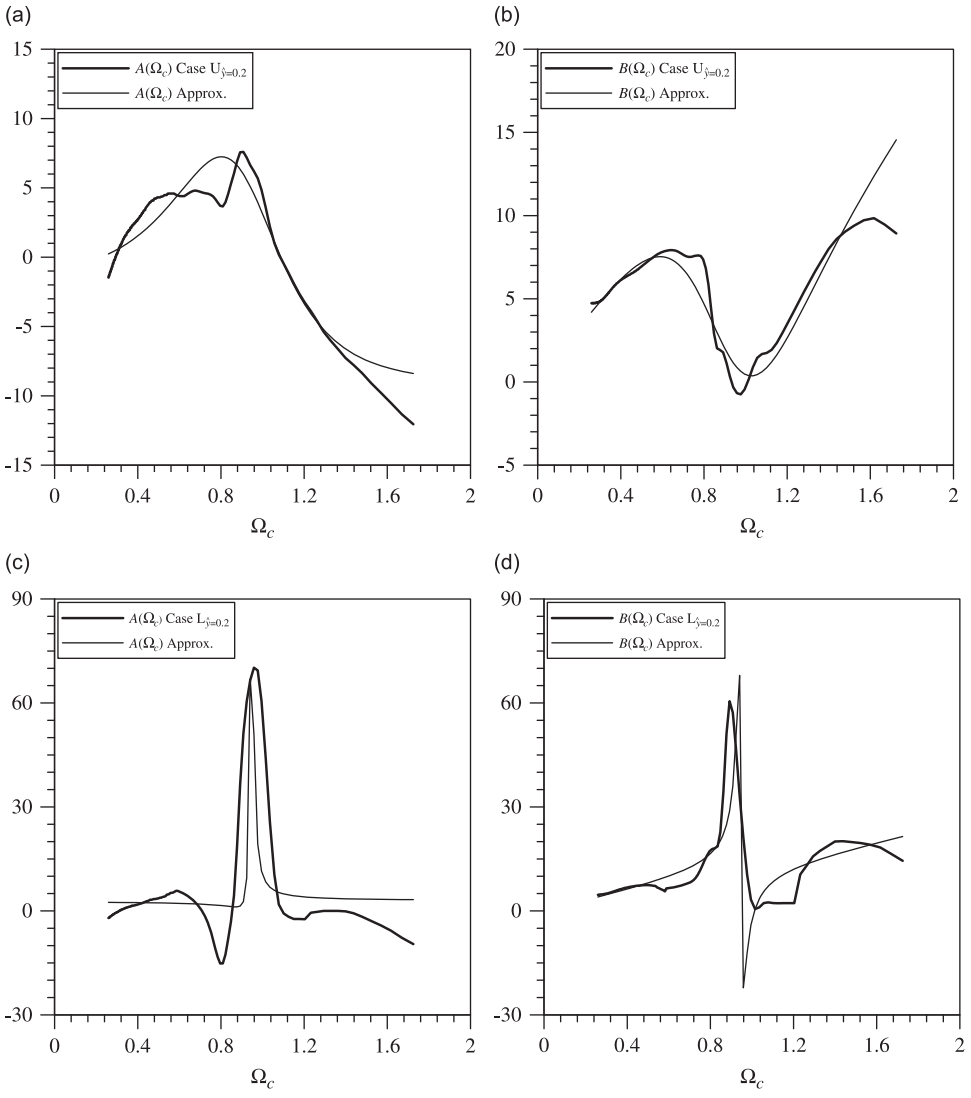

Fig. 9. Best found curve fit for: (a) the coefficient A for $\hat{y} = 0.2$, Case U, (b) the coefficient B for $\hat{y} = 0.2$, Case U, (c) the coefficient A for $\hat{y} = 0.2$, Case L and (d) the coefficient B for $\hat{y} = 0.2$, Case L.

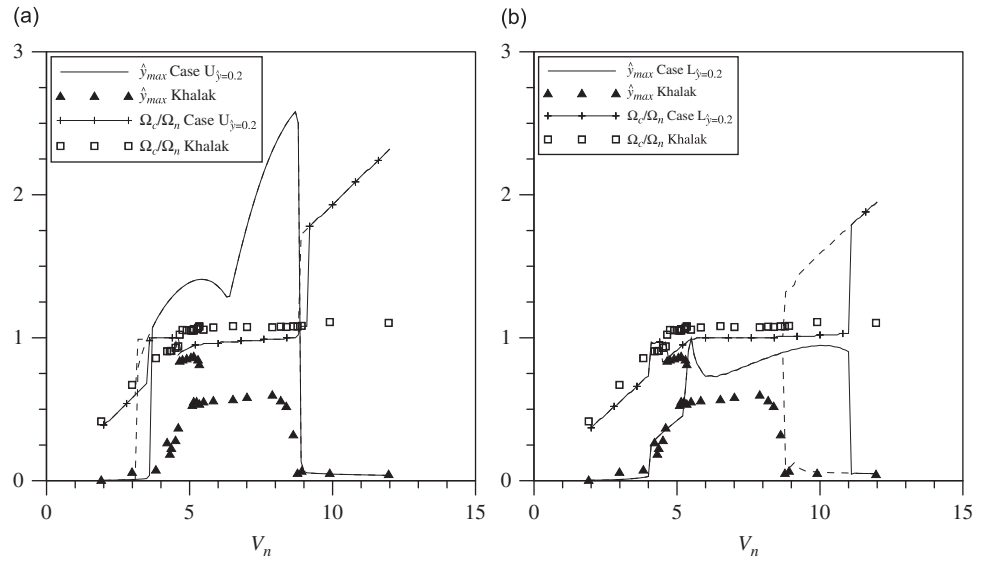

Fig. 10. Comparison of amplitude and frequency of oscillation of the frequency dependent model with the measurements of Khalak et al. [11] for $m^*=10.3$ for: (a) Case U and (b) Case L.

Using the method of Gustavsen and Semlyen, it has first been attempted to fit the average curves of A and B. We did not succeed in finding a fit either for Case U or for Case L. Regardless of the number of poles used, there was always at least one pair of conjugate poles with positive real parts. It was then tried to fit the frequency dependent curves A and B that have been obtained at the eleven amplitudes of forced vibration ($\hat{y}=0.2$, $\hat{y}=0.3$, etc. to $\hat{y}=1.2$) separately, both for Case U and Case L. We did not succeed in finding any fit for the curves of A and B at amplitudes higher than 0.6. For lower amplitudes fitting the curves was only possible by using at most two pairs of conjugate poles ($N=2$). If more poles were used, at least one pair of poles had a positive real part. In all cases in which it was possible to fit the curves with poles with negative real parts, the fit was of poor quality. Examples are given in Fig. 9. In Fig. 9a and b the best fit is shown, that could be obtained for the curves of A and B at an amplitude of 0.2 for Case U and in Fig. 9c and d for Case L. For both cases $N=1$. For Fig. 9a and b, $a_1=-0.3516+\mathrm{i}0.8974$, $c_1=4.7200-\mathrm{i}2.5191$, $d=-9.0431$ and $h=12.8230$. For Fig. 9c and d, $a_1=-0.0101-\mathrm{i}0.9460$, $c_1=0.9200-\mathrm{i}0.2546$, $d=3.0099$ and $h=13.3192$.

Thus, the best that has been achieved in fitting the frequency dependencies of A and B by the admissible functions given by Eq. (55) is a poor fit of the curves that correspond to the lower than 0.6 nondimensional amplitudes. Before drawing conclusions based on this result, it seems reasonable to check the extent to which the free vibration experiment can be reproduced based on this poor fit. To this end the kernel K^* has been determined based on the fit of A and B made at an amplitude of 0.2, see Fig. 9. This kernel is then used in the following final form of the wake oscillator:

$$\ddot{q}+\varepsilon(q^2-1)\dot{q}+q=\int_0^{\tau}K^*(\tau-\tilde{\tau})\dot{y}(\tilde{\tau})\,\mathrm{d}\tilde{\tau}+d\dot{y}+h\ddot{y}, \tag{59}$$

The system of equations given by (20) and (59) has been solved in a manner similar to that explained in Section 3.2, except that now at every time step the integral in Eq. (59) had to be evaluated. The number of previous time steps that needs to be included in the convolution in Eq. (59) depends on the values of a_n and c_n, but it was found that it was not necessary to include the complete tail of the convolution kernel K^*, typically including the last 1000 time steps was sufficient. Although at every time step an integral needs to be evaluated, solving the system did not result in a much longer computational time than when solving the system without the convolution integral. As could already have been expected on the basis of the unsuccessful attempts to fit the curves for A and B, the final results of the modeling of the free vibration were poor. In Fig. 10 the model predictions are compared with the measurements of Khalak and Williamson for $m^*=10.3$. Obviously, both for Case U in Fig. 10a and Case L in Fig. 10b the results are poor.

The results obtained in Sections 5.1 and 5.2 can be summarized as follows. When using the Van der Pol or Rayleigh equation it is not possible to find one set of frequency dependencies $A(\Omega_c)$ and $B(\Omega_c)$ that is valid at all amplitudes of forced vibration. At every amplitude of forced vibration a different set of curves was found. Had the correct nonlinearities been known and used in the governing equations of motion, then only one set of curves would have been found, or even constant values for A and B over the entire frequency range. Thus, the nonlinearities in the chosen oscillator model do not allow accurate reproduction of the results of vortex-induced vibration experiments. This statement will be further discussed in the next section.

6. Concluding remarks

In this paper an attempt has been made to improve a wake oscillator model based on the model of Facchinetti et al. [35] by introducing a frequency dependent coupling. The idea of this improvement arises from the obvious desire to have a model that satisfies both the free and forced vibration experiments.

It is quite easy to check that the existing wake oscillator models describe the forced vibration experiments very poorly. One may hope to remove this discrepancy by introducing frequency dependent coefficients to the model. However, the analysis carried out in this paper has shown that the frequency dependent coefficients found based on the forced vibration experiments are contradictory. First of all, it has been found that it is impossible to find one set of the frequency dependent coefficients that would satisfy the forced experiments at different amplitudes of vibration. Furthermore, we have not succeeded in extending the coefficients from the measured frequency interval to the infinite frequency domain in a non-contradictory manner (in a manner that conforms to the Kramers–Kronig relations). Note that such a non-contradictory extension is absolutely necessary if one aims at having a true time-domain model.

The above findings uniquely suggest that the wake oscillator with the nonlinearities that have been used in this paper cannot accurately reproduce the results of both the forced and free VIV measurements. Such strong conclusion could not have been drawn, had the frequency dependent coefficients not been searched for. This constitutes the main novel result of this paper: to prove the validity of a wake oscillator model one has to require that it describes both the free and forced vibration experiments and then show that the frequency dependent coefficients (which could be, in principle, constant) are non-contradictory. This approach is envisaged to help find the correct nonlinearities of the wake oscillator model in the future.

The importance of gaining understanding in the nonlinearities that are involved in VIV cannot be underestimated. In the force-decomposition method forced vibration measurements are applied directly to the equations of structural motion. If one would wish to extend this method to include in-line motion as well, forced vibration measurements should be performed for at least a four-parameter space, namely cross-flow amplitude and frequency, in-line amplitude and in-line phasing with respect to the cross-flow motion and possibly in-line frequency as well. It is simply impossible to perform the necessary number of tests to cover the entire parameter space. What is needed here is insight in the fundamentals of VIV and any method that can valuate a set of equations that has been proposed is helpful. The results of this paper should be seen in this light.

It is worth noting that the phenomenological model used in this paper has been tuned on measurements and hence all 3D flow effects that were present in the measurements are accounted for by the model. Thus, the 3D distribution of the flow that is vital in the direct numerical modeling of VIV is automatically included in the phenomenological oscillator model. Unfortunately, this is true only for rigid cylinders. The applicability of the model to flexible cylinders may be jeopardized by a different flow distribution along the segments of the flexible cylinder than that observed in the tests with rigid cylinders.

This paper also contains another new and directly applicable result. It has been found that the wake oscillator model based on the model of Facchinetti et al. can be tuned much more easily if the small angle assumption in the cross-flow and in-line vortex forces C_{VY} and C_{VX} given by Eqs. (16) and (28) is not made. The model can then be tuned to the lower branch of free vibration, as can be seen in Fig. 5, but is also able to model the magnification of the mean in-line force for an oscillating cylinder, as can be seen in Fig. 7f. Therefore, the best model at the moment without frequency dependent effects seems to be given by Eqs. (14) and (20) and tuned as in Case L as given by (22).

References

[1] T. Sarpkaya, A critical review of the intrinsic nature of vortex-induced vibrations, *Journal of Fluids and Structures* 19 (2004) 389–447.
[2] C.H.K. Williamson, R. Govardhan, Vortex-induced vibrations, *Annual Review of Fluid Mechanics* 36 (2004) 413–455.
[3] R.D. Gabbai, H. Benaroya, An overview of modeling and experiments of vortex-induced vibration of circular cylinders, *Journal of Sound and Vibration* 282 (2005) 575–616.
[4] T. Sarpkaya, Fluid forces on oscillating cylinders, *Journal of the Waterway, Port, Coastal and Ocean Division* 104 (1978) 275–290.
[5] J.R. Chaplin, P.W. Bearman, F.J. Huera Huarte, R.J. Pattenden, Laboratory measurements of vortex-induced vibrations of a vertical tension riser in a stepped current, *Journal of Fluids and Structures* 21 (2005) 3–24.
[6] J.K. Vandiver, V. Jaiswal, V. Jhingran, Insights on vortex-induced, traveling waves on long risers, *Journal of Fluids and Structures* 25 (2009) 641–653.
[7] L. Mathelin, E. de Langre, Vortex-induced vibrations and waves under shear flow with a wake oscillator model, *European Journal of Mechanics B/Fluids* 24 (2005) 478–490.
[8] R. Violette, E. de Langre, J. Szydlowski, Computation of vortex-induced vibrations of long structures using a wake oscillator model: comparison with DNS and experiments, *Computers and Structures* 85 (2007) 1134–1141.
[9] W.E. Cummins, The impulse response function and ship motions, *Schiffstechnik* 47 (1962) 101–109.
[10] R. Gopalkrishnan, Vortex-induced Forces on Oscillating Bluff Cylinders, Ph.D. Thesis, Massachusetts Institute of Technology, 1992.
[11] A. Khalak, C.H.K. Williamson, Motions, forces and mode transitions in vortex-induced vibrations at low mass-damping, *Journal of Fluids and Structures* 13 (1999) 813–851.
[12] C.C. Feng, The Measurement of Vortex Induced Effects in Flow Past Stationary and Oscillating Circular and D-section Cylinders, M.Sc. Thesis, The University of British Columbia, 1968.
[13] F.S. Hover, A.H. Techet, M.S. Triantafyllou, Forces on oscillating uniform and tapered cylinders in crossflow, *Journal of Fluid Mechanics* 363 (1998) 97–114.
[14] A. Khalak, C.H.K. Williamson, Dynamics of a hydroelastic cylinder with very low mass and damping, *Journal of Fluids and Structures* 10 (1996) 455–472.
[15] A. Khalak, C.H.K. Williamson, Fluid forces and dynamics of a hydroelastic structure with very low mass and damping, *Journal of Fluids and Structures* 11 (1997) 973–982.

[16] J.T. Klamo, A. Leonard, A. Roshko, On the maximum amplitude for a freely vibrating cylinder in cross-flow, *Journal of Fluids and Structures* 21 (2005) 429–434.
[17] J.T. Klamo, A. Leonard, A. Roshko, The effects of damping on the amplitude and frequency response of a freely vibrating cylinder in cross-flow, *Journal of Fluids and Structures* 22 (2006) 845–856.
[18] R.E.D. Bishop, A.Y. Hassan, The lift and drag forces on a circular cylinder in a flowing fluid, *Proceedings of the Royal Society of London. Series A, Mathematical and Physical Sciences* 277 (1964) 32–50.
[19] R.E.D. Bishop, A.Y. Hassan, The lift and drag forces on a circular cylinder oscillating in a flowing fluid, *Proceedings of the Royal Society of London. Series A, Mathematical and Physical Sciences* 277 (1964) 51–75.
[20] J.A. Mercier, Large Amplitude Oscillations of a Circular Cylinder in a Low-speed Stream, Ph.D. Thesis, Stevens Institute of Technology, 1973.
[21] T. Staubli, Untersuchung der oszillierenden Kräfte am querangeströmten, schwingenden Kreiszylinder, Doctoral Thesis, Eidgenössischen Technischen Hochschule Zürich, 1983.
[22] Z.J. Wu, Current Induced Vibrations of a Flexible Cylinder, Doctoral Thesis, Norwegian Institute of Technology, University of Trondheim, 1989.
[23] G. Birkhoff, Formation of vortex streets, *Journal of Applied Physics* 24 (1953) 98–103.
[24] G. Birkhoff, E.H. Zarantonello, in: *Jets, Wakes and Cavities*, Academic Press, New York, 1957.
[25] R.T. Hartlen, I.G. Currie, Lift-oscillator model of vortex-induced vibration, *Proceedings of the American Society of Civil Engineers, Journal of the Engineering Mechanics Division* 96 (1970) 577–591.
[26] R.A. Skop, O.M. Griffin, A model for the vortex-excited resonant response of bluff cylinders, *Journal of Sound and Vibration* 27 (1973) 225–233.
[27] O.M. Griffin, R.A. Skop, G.H. Koopmann, The vortex-excited resonant vibrations of circular cylinders, *Journal of Sound and Vibration* 31 (1973) 235–249.
[28] Y. Nakamura, Vortex excitation of a circular cylinder treated as a binary flutter. Reports of Research Institute for Applied Mechanics, Kyushu University XVII, vol. 59, 1969, pp. 217–234.
[29] Y. Tamura, G. Matsui, Wake-oscillator model of vortex-induced oscillation of circular cylinder, *Proceedings of the Fifth International Conference on Wind Engineering*, Fort Collins, 1979, pp. 1085–1094.
[30] W.D. Iwan, R.D. Blevins, A model for vortex induced oscillation of structures, *Journal of Applied Mechanics* 41 (1974) 581–586.
[31] R. Landl, A mathematical model for vortex-excited vibrations of bluff bodies, *Journal of Sound and Vibration* 42 (1975) 219–234.
[32] E. Berger, On a mechanism of vortex excited oscillations of a cylinder, *Journal of Wind Engineering and Industrial Aerodynamics* 28 (1988) 301–310.
[33] S. Krenk, S.R.K. Nielsen, Energy balanced double oscillator model for vortex-induced vibrations, *Journal of Engineering Mechanics* 125 (1999) 263–271.
[34] R.A. Skop, S. Balasubramanian, A new twist on an old model for vortex-excited vibrations, *Journal of Fluids and Structures* 11 (1997) 395–412.
[35] M.L. Facchinetti, E. de Langre, F. Biolley, Coupling of structure and wake oscillators in vortex-induced vibrations, *Journal of Fluids and Structures* 19 (2004) 123–140.
[36] E. de Langre, Frequency lock-in is caused by coupled-mode flutter, *Journal of Fluids and Structures* 22 (2006) 783–791.
[37] R.D. Blevins, in: *Flow-Induced Vibration*, second ed, Krieger Publishing Company, Malabar, 2001.
[38] B.M. Sumer, J. Fredsøe, in: *Hydrodynamics Around Cylindrical Structures*, World Scientific Publishing, Singapore, 1997.
[39] W.C. Elmore, M.A. Head, in: *Physics of Waves*, Dover Publications, New York, 1985.
[40] A.T. de Hoop, in: *Handbook of Radiation and Scattering of Waves*, Academic Press, London, 1995.
[41] W.H. Press, S.A. Teukolsky, W.T. Vetterling, B.P. Flannery, in: *Numerical Recipes in Fortran 77: The Art of Scientific Computing*, second ed, Cambridge University Press, Cambridge, 1992.
[42] E.C. Levy, Complex-curve fitting, *IEEE Transactions on Automatic Control* 4 (1959) 37–44.
[43] C.K. Sanathanan, J. Koerner, Transfer function synthesis as a ratio of two complex polynomials, *IEEE Transactions on Automatic Control* 9 (1963) 56–58.
[44] B. Gustavsen, A. Semlyen, Rational approximation of frequency domain responses by vector fitting, *IEEE Transactions on Power Delivery* 14 (1999) 1052–1061.